Science of the Total Environment 776 (2021) 145934

Contents lists available at ScienceDirect

Science of the Total Environment

journal homepage: www.elsevier.com/locate/scitotenv

# Zinc removal and recovery from industrial wastewater with a microbial fuel cell: Experimental investigation and theoretical prediction

Swee Su Lim [a,c], Jean-Marie Fontmorin [a], Hai The Pham [d], Edward Milner [a], Peer Mohamed Abdul [e], Keith Scott [a], Ian Head [b], Eileen Hao Yu [a,f,*]

[a] School of Engineering, Newcastle University, Newcastle upon Tyne NE1 7RU, United Kingdom
[b] School of Natural and Environmental Sciences, Newcastle University, Newcastle upon Tyne NE1 7RU, United Kingdom
[c] Fuel Cell Institute, Universiti Kebangsaan Malaysia, 43600 UKM, Bangi, Malaysia
[d] Department of Microbiology and Center for Life Science Research (CELIFE), Faculty of Biology, VNU University of Science, Vietnam National University, 334 Nguyen Trai, Thanh Xuan, Hanoi, Vietnam
[e] Department of Chemical and Process Engineering, Faculty of Engineering and Built Environment, Universiti Kebangsaan Malaysia, 43600 UKM, Bangi, Selangor, Malaysia
[f] Department of Chemical Engineering, Loughborough University, Loughborough LE11 3TU, United Kingdom

## HIGHLIGHTS

- More than 96% of $Zn^{2+}$ was successfully removed in batch mode MFC.
- The $Zn^{2+}$ concentration of 2 mM was reduced to 0.07 mM within 22 h of MFC operation.
- Hydroxide was produced by oxygen reduction and used in $Zn^{2+}$ removal process.
- Approximately 83% of the recovered $Zn^{2+}$ was attached to the cathode from synthetic wastewater.
- The $Zn^{2+}$ removal in MFC mode can be modelled by using first order reaction rate.

## GRAPHICAL ABSTRACT

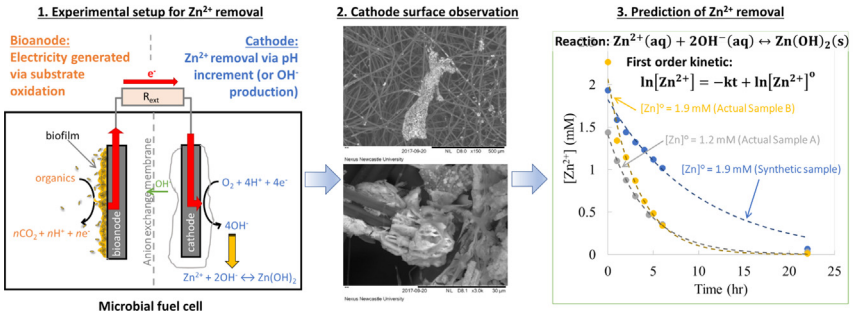


## ARTICLE INFO

*Article history:*
Received 16 November 2020
Received in revised form 11 February 2021
Accepted 11 February 2021
Available online 19 February 2021

Editor: Yifeng Zhang

*Keywords:*
Zinc removal
Heavy metal recovery
Microbial fuel cell
Theoretical and mathematical modelling
Electroprecipitation
Industrial wastewater treatment

## ABSTRACT

Microbial fuel cells (MFCs) that simultaneously remove organic contaminants and recovering metals provide a potential route for industry to adopt clean technologies. In this work, two goals were set: to study the feasibility of zinc removal from industrial effluents using MFCs and to understand the removal process by using reaction rate models. The removal of $Zn^{2+}$ in MFC was over 96% for synthetic and industrial samples with initial $Zn^{2+}$ concentrations less than 2.0 mM after 22 h of operation. However, only 83 and 42% of the zinc recovered from synthetic and industrial samples, respectively, was attached on the cathode surface of the MFCs. The results marked the domination of electroprecipitation rather than the electrodeposition process in the industrial samples. Energy dispersive X-ray (EDX) analysis showed that the recovered compound contained not only Zn but also O, evidence that $Zn(OH)_2$ could be formed. The removal of $Zn^{2+}$ in the MFC followed a mechanism where oxygen was reduced to hydroxide before reacting with $Zn^{2+}$. Nernst equations and rate law expressions were derived to understand the mechanism and used to estimate the $Zn^{2+}$ concentration and removal efficiency. The zero-, first- and second-order rate equations successfully fitted the data, predicted the final $Zn^{2+}$ removal efficiency, and suggested that possible mechanistic reactions occurred in the electrolysis cell (direct reduction), MFC ($O_2$ reduction), and control (chemisorption) modes. The half-life, $t_{1/2}$, of the $Zn^{2+}$ removal reaction using synthetic and industrial samples was estimated to be 7.0 and 2.7 h, respectively. The $t_{1/2}$ values of the controls (without the power input

* Corresponding author at: School of Engineering, Newcastle University, Newcastle upon Tyne NE1 7RU, United Kingdom.
*E-mail address:* e.yu@lboro.ac.uk (E.H. Yu).

https://doi.org/10.1016/j.scitotenv.2021.145934

from the MFC bioanode) were much slower and were recorded as 21.5 and 7.3 h for synthetic and industrial samples, respectively. The study suggests that MFCs can act as a sustainable and environmentally friendly technology for heavy metal removal without electrical energy input or the addition of chemicals.



## 1. Introduction

Zinc has a variety of applications, such as in corrosion-resistant coatings, dry-cell batteries, alloys, paints, plastics, rubber, dyes, wood preservatives and cosmetics. The origin of man-made pollution is mainly from metal production processes, industrial combustion of coal, waste incineration and worn rubber tires on vehicles (S.E.P.A., 2018; Modestra et al., 2017). Studies have shown that out of 162 wastewater treatment plants in the UK, in 50% of cases, the level of zinc in the effluent stream was higher than the recommended level set by the Environment Agency (0.017 ppm or 0.26 mM) (W.F.D., 2013). Discharging zinc-containing wastewaters into natural environments can significantly affect local aquatic ecosystems. Several treatment methods have been used to remove heavy metals from wastewater streams. However, most of these methods, such as chemical precipitation and coagulation-flocculation, are only reliable when treating high concentrations of heavy metals (e.g., >1000 ppm) and require the usage of chemical reagents. These methods not only increase the cost of operation but also the complexity of the treatment of wastewaters, as secondary by-products are generated during the treatment and require further disposal (Fu and Wang, 2011). Although other methods, such as ion exchange and membrane filtration, can effectively remove heavy metal ions from targeted wastewaters, they are energy intensive, and their maintenance is expensive (Dominguez-Benetton et al., 2018). Therefore, an effective but low-cost method is necessary for treating wastewaters containing medium to low concentrations of metals.

The utilisation of microbial fuel cells (MFCs) to remove or recover heavy metals from waste streams and soils has been studied in recent years (Modestra et al., 2017; Dominguez-Benetton et al., 2018; Nancharaiah et al., 2015). The system is based on electrochemically active microbes at the anode (called the bioanode) to not only provide reducing potential to support the cathode in metal reduction but also to treat wastewaters by oxidising the organic matter. However, there is a limitation in the system, as the bioanode could only provide the reduction potential down to approximately −0.20 V vs. standard hydrogen electrode (SHE) under optimal conditions (Lim et al., 2017). This limitation restricts the spontaneous treatment of certain metals, e.g., $Cu^{2+}$, $Cr^{6+}$, $V^{5+}$, and $Fe^{3+}$, whose reduction potentials are higher than −0.20 V vs. SHE. While most heavy metal ion reduction potentials are lower than this value, e.g., $Cr^{3+}$, $Cd^{2+}$, $Ni^{2+}$ and $Zn^{2+}$, external energy is required to further lower the cathode potential. As direct reduction of metal ions is impossible to achieve, hydroxide precipitation is an alternative option using MFCs (Fang and Achal, 2019). The working principle of the MFC is totally environmentally friendly and natural, as no chemical is required during the precipitation process since the bioanode (enriched from natural habitat) is used to assist hydroxide production at the cathode. Energy recovered from wastewater via electrochemical reaction of the bioanode is then re-channelled to the cathode to support metal precipitation (Wang et al., 2016a). The energy cycle makes the MFC attractive and promising, as no external energy or additional chemicals are required during the entire process. Moreover, the objective also supports the United Nations agenda in transforming the world for Sustainable Development during 2030, especially under Goal 7: Affordable and Clean Energy and Goal 12: Responsible Consumption and Production.

Table 1 shows the summary and development of $Zn^{2+}$ removal methods using bioelectrochemical systems. As depicted in the table, most of the studies required the assistance of an external power supply and used only synthetic $Zn^{2+}$-containing wastewater in their studies.

**Table 1**
$Zn^{2+}$ removal using the bioelectrochemical system.

| Applied voltage, $V_{ap}$ (V) | Max. current, $I_{max}$ ($A/m^2$) | Max. power, $P_{max}$ ($W/m^2$) | Initial $[Zn^{2+}]$ (mM) | Removal efficiency (%) | Removal period, t (hr) | Catholyte H[a] | Category[b] | Note | Reference |
|---|---|---|---|---|---|---|---|---|---|
| 0.75 | 1.08 | N.P. | 12.24 | 99 | 1 | 4 | A | Only $Zn^{2+}$ was focused upon and studied. | (Modin et al., 2017) |
| 0.7 | 50 | 35 | 0.23–0.38 | 99 | 48 | 3.0 → 6.6 | D | *Desulfovibrio* sp. dominated **biocathode** was enriched for treating $Zn^{2+}$ and $SO_4^{2-}$ (2.08 mM). | (Teng et al., 2016) |
| 0.472 | 0.786 | 0.372 | 6.12 | 93 | 72 | 5.35 → 2.19 | X | $Zn^{2+}$ was recovered by **stripping chamber** with a supported liquid membrane attached next to cathode chamber. | (Fradler et al., 2014) |
| 0.316 | 11.7 | 3.6 | 0.20 | 97 | 40 | 6.8 → 7.1 | X | Both $Zn^{2+}$ and $Cd^{2+}$ (0.40 mM) were treated by the same **anode** of a **single chamber MFC**. | (Abourached et al., 2014) |
| 0.8 | 1.689 | 1.35 | 4.59 | 44.2 | 2 | ≈0 (2 M HCl) | A | $Cu^{2+}$ (12.6 mM), $Pb^{2+}$ (1.93), $Cd^{2+}$ (7.12) and $Zn^{2+}$ were tested in the same setup and recovered by controlling the **cell potential** in a **sequential procedure**. | (Modin et al., 2012) |
| 6.0 | 90 | N.P. | 2.75 | 95.4 | 10 | 7 | A | $Cu^{2+}$ (0.82 mM) and $Pb^{2+}$ (0.48) were removed in the same chamber under **MFC mode** followed by **electrolysis process**. | (Tao et al., 2014) |
| 0.05[c] | 1.17 | N.P. | 0.46 | 91.5 | 20 | 7 | B | **Two MFCs** operated in parallel under the **change and discharge cycles**. $Cu^{2+}$ (0.47 mM) and $Cd^{2+}$ (0.27) were also tested but in a separated setup. | (Wang et al., 2016b) |
| 0[c] | 0.15 | N.A. | 2.00 | 96 | 22 | 6.0 → 8.4 | B | $Zn^{2+}$ was focused and studied by using **INDUSTRIAL** and synthetic samples. **MATHEMATICAL** models were used to explain the mechanistic process | This study |

N.P. – Not provided. N.A. – Not available.

[a] Initial pH value. The arrow sign indicates the changes in pH value between inlet/outlet or before/after treatment.

[b] Based on Dominguez-Benetton et al. (Dominguez-Benetton et al., 2018): Category A – A biological anode coupled to direct electrochemical metal reduction on an abiotic cathode, Category B – A biological anode coupled to electrochemical generation of reductants at the cathode, Category C – A biological anode coupled to a cathode compartment with electrochemical metal reduction and (bio)chemical reoxidation, category D – systems with a biological cathode, and X – other type of systems.

[c] Cell voltage during $Zn^{2+}$ removal operated under MFC mode.

They include supported liquid membranes and extra strip chambers to separate and concentrate $Zn^{2+}$ (Fradler et al., 2014), treating organic and $Zn^{2+}$-containing wastewater in anode chambers under biosorption and sulfide precipitation mechanisms (Abourached et al., 2014), and directly reducing $Zn^{2+}$ to metallic Zn at the cathode with the assistance of external energy input (Modin et al., 2012; Tao et al., 2014; Modin et al., 2017). These studies have provided insightful information on the potential of bioelectrochemical systems (BESs), especially microbial fuel cells (MFCs) and microbial electrolysis cells (MECs), for $Zn^{2+}$ removal. Nevertheless, to better assess the viability of MFCs for zinc recovery from industrial effluents, especially without the assistance of any external power supply, more studies should be carried out with actual effluents and containing lower and more representative $Zn^{2+}$ concentrations. Other than the real application aspect, the results also required estimation of the reaction kinetics to better predict the removal of the metals within a specific time and under specific conditions. The equivalent ratios and rates in scale-up applications must be derived from mathematical modelling and used during the application process. To date, few studies have used rate reaction models in the prediction of MFC-based metal ion removal and thus provide little information regarding the prediction of $Zn^{2+}$ removal.

The aim of this work is to study and predict the effectiveness of MFCs for the removal of $Zn^{2+}$ from actual industrial effluents. In addition to understanding the practicality of the process, the reaction rate is applied to determine the reaction kinetics and to predict the plausible pathways of the overall process. In the first part of the study, experiments were carried out to evaluate the potential of MFCs for $Zn^{2+}$ removal from actual industrial effluents. In the second part, a Pourbaix diagram was used to predict the mechanistic process of $Zn^{2+}$ removal. In addition, the Nernst equation was used to calculate the equilibrium potential and the driving force potential that could be provided by the MFC to remove $Zn^{2+}$. Mathematical models were also derived according to the law of rate reaction to predict the reaction behaviour, required time and feasibility of $Zn^{2+}$ removal in MFCs.

## 2. Methods and materials

### 2.1. Half-cell experiment

The study was started with half-cell setup (without a bioanode). The setup consisted of an abiotic anode and cathode separated by an anion exchange membrane (AEM) (FAB-PK-130, Fumasep, Fumatech, Germany) (Fig. 1(a)). Both anodic and cathodic chambers were identically fabricated from clear Perspex with an internal working volume of $7 \times 7 \times 2$ $cm^3$. Inlets and outlets at the sides of the chambers were prepared for inflow and outflow of electrolytes. A push-in fitting was installed, and an extra hole was prepared on the top of the chambers to accommodate reference electrodes and to connect the electrodes to external connections. Both electrodes were plain carbon felts with an active projected area of $3 \times 3$ $cm^2$ bolted at the internal space of the chambers.

The anolyte consisted of 1.0 g/L sodium acetate, while the catholyte consisted of 1.9 mM $ZnCl_2$. Both electrolytes were added to 3.0 g/L NaCl to increase their initial conductivity in solution. A range of fixed currents (galvanostatic method) up to 5.56 $A/m^2$ was applied to the BES for 180 min using a potentiostat (PGSTAT128N, Metrohm, Netherlands). The cell voltage was recorded every 10 s. The changes in pH were logged using a pH meter (Accumet AB150, Fisher brand, USA) every 5 min. Meanwhile, anolyte and catholyte samples (5.0 mL) were collected every 30 min and kept at 4 °C prior to analysis. The acetate concentration was analysed by gas chromatography (Tracera GC-2010 Plus, Shimadzu, UK) equipped with a barrier ionisation discharge (BID) detector. The $Zn^{2+}$ concentration was determined by inductively coupled plasma optical emission spectrometry (ICP-OES) (Optima 8000, Perkin Elmer, USA). All tests were conducted at room temperature (22 ± 3 °C).

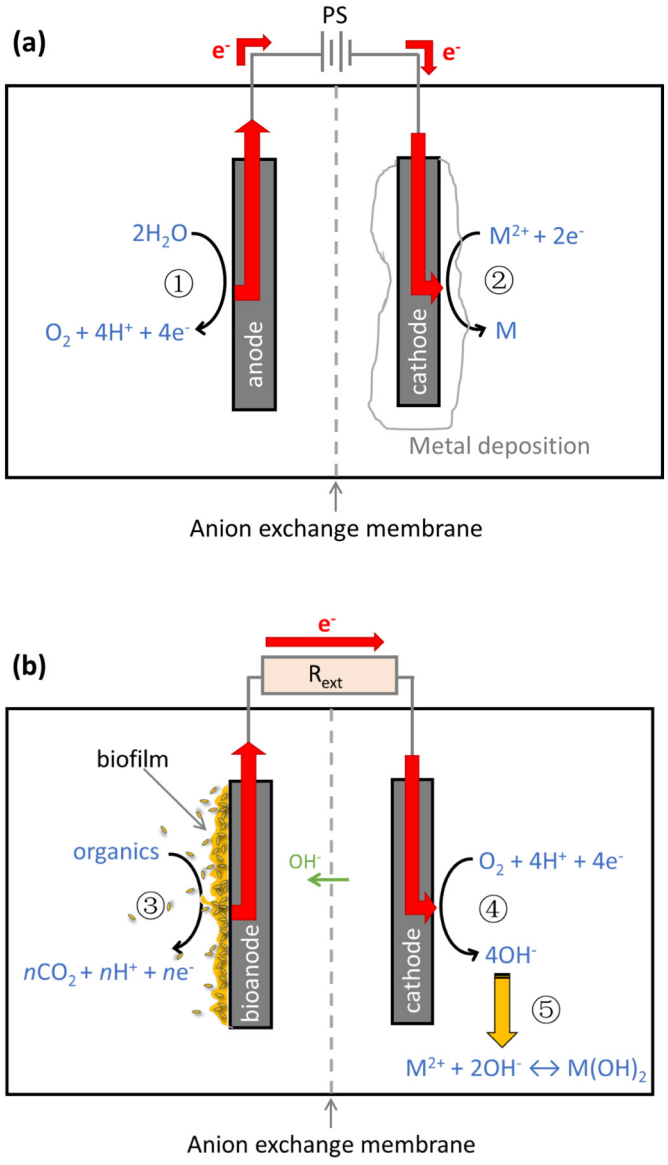


**Fig. 1.** Schematics of the bioelectrochemical systems: (a) electrolysis cell and (b) microbial fuel cell. Note that the power supply (PS) in (a) is replaced by the external resistance ($R_{ext}$) in (b). Reaction ①: water electrolysis, Reaction ②: metal ion reduction, Reaction ③: substrate oxidation, Reaction ④: oxygen reduction reaction (ORR), and Reaction ⑤: metal ion precipitation.

### 2.2. Zinc removal operation

After an optimal operating condition was identified from the study in Section S1, the Pt cathode was replaced with plain graphite felt for the zinc removal study. There are a few reasons for replacing the Pt cathode with a new plain cathode in this study: (1) reducing Pt interference as zinc deposition might block the catalysis function, (2) providing a control condition without Pt interference, (3) avoiding the usage of expensive catalysts, and (4) focusing on studying bioanode performance in $Zn^{2+}$ removal under standalone operating conditions. In addition to monitoring potentials, electrolyte pH and $Zn^{2+}$ concentration were recorded and determined as described in Section S1 unless stated otherwise. At the end of the process, the MFC was dismantled, and the cathode was subjected to scanning electron microscopy (SEM) and energy dispersive X-ray spectroscopy (EDX) imaging to study the surface morphology and zinc deposition properties.

### 2.3. Data collecting and samples analysis

#### 2.3.1. Potential monitoring and current calculation

Cell and electrode potentials (V) were collected through an 8-channel data logger (ADC-24 data logger, Pico Technology, UK). The cell potential was recorded between the anode and cathode, and electrode potentials were collected by referring to a reference electrode (RE-5B, BASi, US) located in each chamber. All electrode potentials were converted to standard hydrogen electrode (vs. SHE) values. The current density, $I_D$ (A/$m^2$), was calculated from the values of the cell potential, $V_{cell}$ (V) and external resistance, $R_{ext}$ (Ω), by using the formula $I_D = V_{cell} / (R_{ext} \times A_c)$, where $A_c$ ($m^2$) is the projected area of the cathode.

#### 2.3.2. Concentration of metal ions and solution properties

Metal ions and other cations were analysed using an inductively coupled plasma (ICP) system (Optima 8000, Perkin Elmer, USA). To quantify total zinc recovery, the zinc deposited on the cathode was soaked in 2% $HNO_3$ overnight, and the effluent was filtered with a 0.2 μm syringe filter prior to analysis.

Acetate was analysed using a gas chromatograph (Tracera GC-2010 Plus, Shimadzu, UK) equipped with a barrier ionisation discharge (BID) detector (280 °C) and autosampler (AOC-20i, Shimadzu, UK). A column (Zebron ZB-WAX-Plus capillary column 30 m × 0.25 mm × 0.25 μm, Phenomenex, UK) was used to quantify the compound and was operated with a temperature profile of 50 °C for 1 min, ramping to 180 °C at 30 °C/min, then holding at 180 °C for 8 min. The injection port was set at 180 °C with a split ratio of 10:1 under a 1.0 μL injection sample, while the detector was maintained at 280 °C. The carrier gas was high purity grade helium (99.999% BOC, UK) and was maintained at a constant flow rate of 2.0 mL/min. All samples were filtered with 0.2 μm syringe filters and then acidified with HCl 1.0 M at a ratio of 20:1 prior to analysis.

pH and conductivity were measured with a portable pH meter (HI9025 microcomputer pH meter, Hanna Instruments, UK) and conductivity meter (FE30 FiveEasy, Mettler Toledo, USA).

#### 2.3.3. Cathode surface morphology and composition

After each experiment, the cathode surface morphology was analysed by a Hitachi TM3030 scanning electron microscope (SEM) equipped with a Bruker Quantax 70 EDX system. For sample preparation, a 1 cm × 1 cm piece was sliced off the cathode, washed gently with deionized water and dried on a Petri dish overnight at room temperature prior to analysis.

## 3. Results and discussion

### 3.1. Preliminary tests: $Zn^{2+}$ removal in half-cells via direct electrolysis process

Before studying the removal of $Zn^{2+}$ in microbial fuel cells, preliminary tests were carried out in half-cells (using an external power supply) to experimentally quantify the dependence of $Zn^{2+}$ reduction kinetics on applied current and anaerobic (without oxygen) conditions. Fig. 2 shows the evolution of cell voltages, pH and $Zn^{2+}$ concentration in half-cells. All tests were done within 180 min. When the applied current was increased, the cell voltage and the pH increased, as presented in Fig. 2(a) and (b), respectively. However, it should be noted that only the two highest current densities applied led to a measurable change in pH in the catholyte. For comparison at 5.56 A/$m^2$, the pH of the catholyte increased from 7.5 to 11.0 in just 80 min, whereas at 2.22 A/$m^2$, the pH increased to 9.0 only at the end of the 180 min of experiment (Fig. 2(b)).

The removal of $Zn^{2+}$ measured at different applied current densities (Fig. 2(c)) was consistent with the trend observed for the catholyte pH. Indeed, complete soluble $Zn^{2+}$ removal (>99%) was observed after 80 and 180 min at current densities of 5.56 and 2.22 A/$m^2$, respectively. Although no significant change in pH could be observed at applied current densities of 0.56 and 0.22 A/$m^2$, $Zn^{2+}$ removal of 15% and 21% could be measured after 180 min of the experiment. This could be explained by a local change in pH, i.e., in the vicinity of the cathode rather than in the bulk when higher current densities are applied. The local change in pH was negligible at a lower current, as $OH^-$ diffusion into the bulk electrolyte was faster than $OH^-$ production at the cathode surface. However, under a higher current, a localised pH change occurred on the cathode surface as $OH^-$ accumulated in the vicinity and diffused slowly into the bulk electrolyte. The results show a direct correlation between the applied current density, the increase in pH in the catholyte and the rate of $Zn^{2+}$ removal. As the current increases, so does the pH due to the production of $OH^{\cdot}$ and in turn, the removal rate of $Zn^{2+}$ increases. Although the best results were obtained at current densities (2.22 and

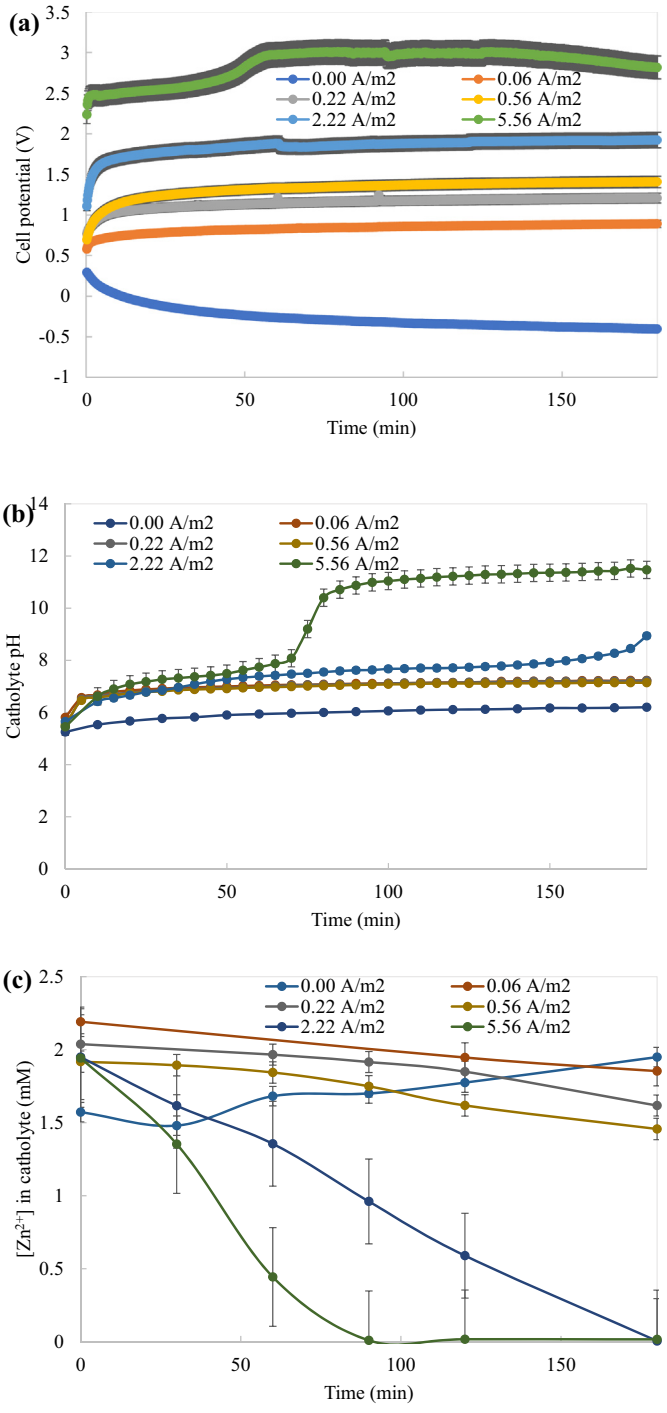


**Fig. 2.** Profiles of (a) cell potential, (b) catholyte pH and (c) $Zn^{2+}$ removal in the electrolysis process under different applied currents.

5.56 A/m$^2$), which are not achievable by conventional bioanodes, it was also observed that removal could be achieved at more realistic current densities. However, experiments would have to be performed for more than 180 min to reach the desired final concentration. Finally, it should be noted that only a small amount of $Zn^{2+}$ was detected in the anolyte, showing that the crossover was negligible (<2% of initial $Zn^{2+}$ in the catholyte) (see Supplementary materials: Fig. S3 (a)).

### 3.2. Zinc recovery from synthetic wastewater

Fig. 3 presents the profiles of cells, electrode potentials and current density in conjunction with $Zn^{2+}$ concentration and pH during zinc recovery from synthetic wastewater. As shown in Fig. 3(a), the control potential (open circuit condition without any load or resistor connected between anode and cathode) was ~0.55 V. In contrast, the cell voltage recorded was approximately a few millivolts when a resistor was connected between the anode and cathode. Under the load condition, the anode started to support the cathodic reduction process at −0.13 V (anodic batch mode) or −0.08 V (anodic flow-through mode) as commonly observed (Dominguez-Benetton et al., 2018; Fang and Achal, 2019; Wang et al., 2016a; Wang et al., 2018; Rodenas Motos et al., 2015). The same phenomenon of lowering the cathode potential was observed when both the anode and cathode were connected through a power supply (Modin et al., 2012; Zhang et al., 2015). The bioanodes used in the experiments were pre-enriched, tested and optimised as mentioned in Section S1 to obtain the best operating conditions (see Supplementary materials: Section S1). At the end of the enrichments, the bioanode generated approximately 2.0–3.0 A/m$^2$ of maximum current density with a 10 Ω resistor connected between the anode and cathode. The operating bioanode recorded a minimum potential at +0.09 V vs. SHE with the cathode potential being +0.10 V, which was higher than the anode potential. Meanwhile, Fig. 3(b) shows that no current was recorded in the control. The MFC operating under the load showed specific electron flow; however, the current recorded in anodic batch mode was slightly higher than that recorded in anodic flow-through mode at the beginning of the process, showing that the mass transport did not limit the anodic reaction. Indeed, the oxidation reaction in the bioanode is slow due to microbial activity; therefore, the mass transport limitation is not an issue under high substrate concentrations (Daud et al., 2018; Lee and Huang, 2013).

$Zn^{2+}$ concentration and pH were also monitored in the cathode, as exhibited in Fig. 3(c). $Zn^{2+}$ concentrations decreased throughout the whole process, while the pH values increased within 2 to 3 h before stabilising. Surprisingly, the $Zn^{2+}$ concentration in the control (anodic batch mode) catholyte also decreased but at a much slower rate than that in the MFC with the load resistor. It is suspected that the components in the control were able to adsorb $Zn^{2+}$ from the catholyte, especially started with new carbon felt and membrane, due to their surface properties (Lefebvre et al., 2012; Luo et al., 2015). Adsorption of $Zn^{2+}$ on the surface of materials can occur particularly when retained materials are negatively charged (Bankole et al., 2019a). Active functional groups in the membrane might react with metal ions and cause metal fouling by forming van der Waals interactions (Dominguez-Benetton et al., 2018; Lu et al., 2015). In addition, as from the Pourbaix diagram (see Section 3.4.1: Fig. 9), a critical demarcation line lays between soluble $Zn^{2+}$ and insoluble $Zn(OH)_2$ at pH 7.0 and for lower (1 mM) $Zn^{2+}$ concentrations. The pH slightly increased, which could have led to $Zn^{2+}$ precipitation. A white precipitate was observed at the bottom of the cathodic chamber at the end of the control experiment. The anodic batch mode MFC had the best performance, and the $Zn^{2+}$ removal was 96% (0.07 mM $Zn^{2+}$ remained in the catholyte) at the end of the experiment compared to the anodic flow-through mode MFC at approximately 80% (0.39 mM $Zn^{2+}$ remained in the catholyte). Under anodic batch mode conditions, power generation is vigorous and concentrated on the available substrate contained in a specified anodic chamber. Each bioanode cycle was beneficial to $Zn^{2+}$ removal, as a focused peak current could create a short electrical surge to increase the $Zn^{2+}$ reduction activity in the cathode. Bioanodes consist of microbes, and extracellular polymeric substances (EPSs) work as capacitive materials that simultaneously produce and store electricity. As a result, larger portion of the electricity in the bioanode can be generated and released under anodic batch condition than in the continuous mode where a stable substrate degradation process is occurred (Wang et al., 2018). As the $Zn^{2+}$ removal value of the control was significant (52% or equal to 0.91 mM)

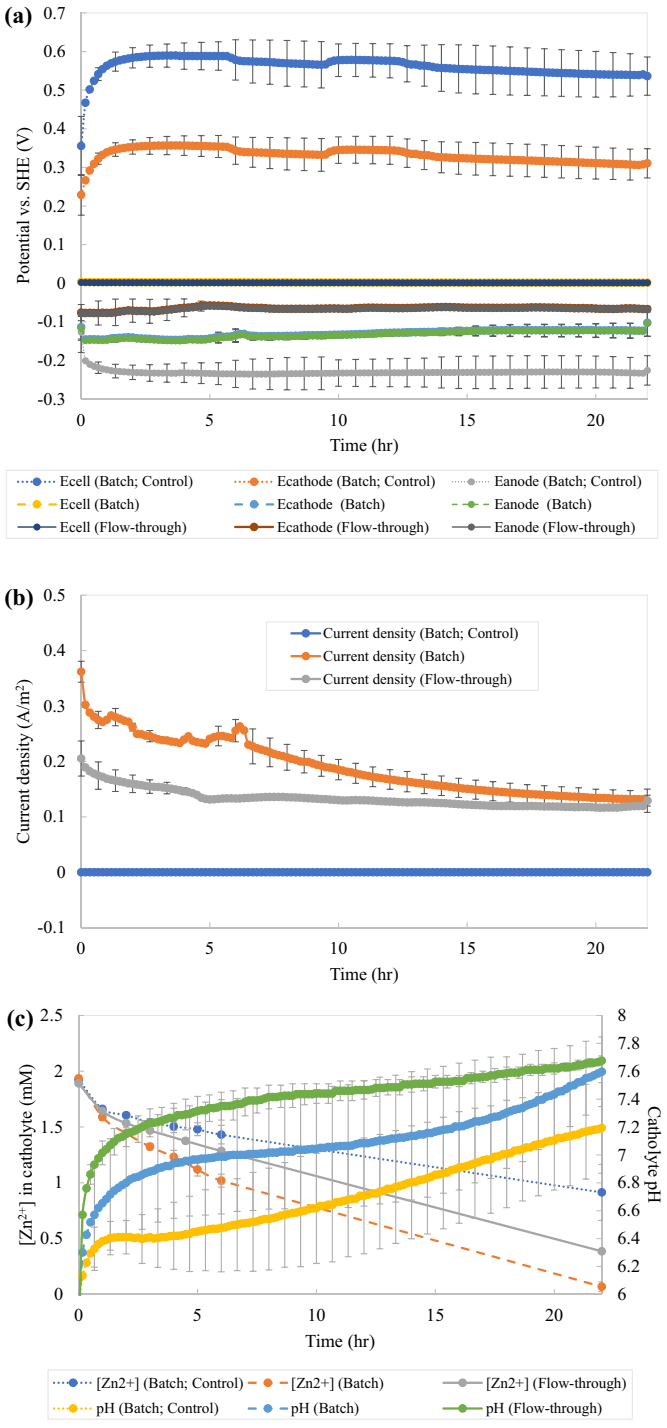


**Fig. 3.** Zinc recovery in MFCs using synthetic wastewater: (a) cell and electrode potentials, (b) current density, and (c) $Zn^{2+}$ concentration and catholyte pH. Note: Control: MFC is operated under open circuit conditions; 10 Ω: MFC is operated with a 10 Ω resistance connected between the anode and cathode; batch: anode is operated in batch mode; flow-through: anolyte is recycled through the anodic chamber with a flow rate of 1 mL/min.

in this experiment, it is important to set the control as a reference to compensate for the interferences from adsorption and/or oxygenation for further interpretations. Further discussion of these matters is continued in Section 3.4.3. The removal rate of the anodic batch mode MFC was also the highest (6.0 mmol/$m^2$ cathode/h), followed by the anodic flow-through MFC (4.0 mmol/$m^2$ cathode/h) and control (2.3 mmol/$m^2$ cathode/h) (the removal rate was calculated from the linear slope of $Zn^{2+}$ concentration between 2 and 5 h using the data presented in Fig. 3(c)).

Fig. 4 exhibits the $Zn^{2+}$ removal and recovery efficiency from the MFC system. It was determined that 96% of $Zn^{2+}$ was removed from the catholyte in anodic batch mode MFC compared to only 52% removal in the control. The anodic flow-through mode MFC had a lower removal efficiency, which was approximately 80%. The adsorption behaviour of the newly replaced materials, as discussed in Section 3.4.3, may have affected $Zn^{2+}$ removal in the controls. The amount of zinc precipitated on the electrode was compared to the total amount of $Zn^{2+}$ removed from the catholyte, and the results are gathered in Fig. 4. The difference between zinc recovered from the electrode and the total $Zn^{2+}$ concentration removed from the catholyte corresponds to the precipitation of Zn $(OH)_2$ directly in the medium. For the anodic batch and flow-through modes under load resistor conditions, the differences between zinc precipitated at the cathode and $Zn^{2+}$ removed from the catholyte are small, i.e. approximately 17 and 7%, respectively (or in other words, cathodic recoveries as $Zn(OH)_2$ in the anodic batch and flow-through modes are approximately 83 and 93%, respectively), showing that most zinc can be recovered from the electrode. However, in the control (anodic batch mode), the difference is as high as 92%. The results confirmed the importance and assistance of the bioanode in cathodic $Zn^{2+}$ removal by electroprecipitation instead of the electrodeposition process.

The cathode surfaces were characterised by SEM/EDX, and the results are presented in Fig. 5. From scanning electron microscopy images, crystals can be observed on the cathode surface, especially under anodic batch mode conditions (Fig. 5(b)). A more homogeneous coverage of Zn species onto the electrode surface was noticed under anodic flow-through mode conditions (Fig. 5(c)), which can be explained by a better diffusion of $Zn^{2+}$ towards the carbon felt. Crystals were also found in the control (Fig. 5(a)); however, they appeared less thick and homogeneous than on the cathodes connected with the 10 Ω resistor. The structure of the crystals depends on the nature of the metal formed during the reduction process (Zhang et al., 2015; Zhang et al., 2012; Huang et al., 2013). For example, polyhedral structures were mainly observed for copper compounds at the end of the experiments (8–9 days) as Cu and $CuO_2$ deposited on the cathode surface at pH 3.0 and with the temperature controlled between 20 and 30 °C (Rodenas Motos et al., 2015; Ter Heijne et al., 2010). From the energy dispersive X-ray spectroscopy

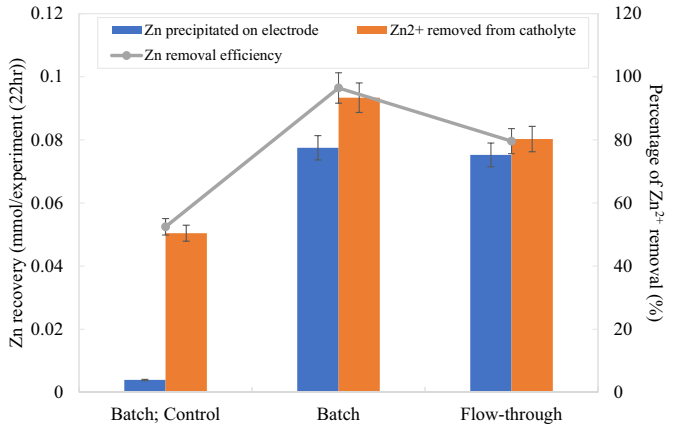


**Fig. 4.** Zinc recovery from the cathode, total removal from the catholyte and removal efficiency in MFCs using synthetic wastewater.

images presented in Fig. 5 (EDX section), it can be seen that the elements C, O and Zn were present on the cathode surfaces, which is consistent with the formation of $Zn(OH)_2$. It can be observed from the EDX figures that Zn and O were evenly distributed on the carbon fibre surface of all samples. However, the EDX signal intensities for Zn and O were slightly higher in anodic batch mode (Fig. 5(b)) than in anodic flow-through mode (Fig. 5(c)). In addition, the element O was co-found in the locations where Zn appeared, indicating evidence of zinc oxide species. From the observation in Fig. 3(b), final catholyte pH values were recorded to be greater than 7.6. The alkaline environment created suitable conditions for the formation of $Zn(OH)_2$ according to the Pourbaix diagram presented in Fig. 9.

### 3.3. Zinc recovery with actual industrial wastewater

After showing the feasibility of zinc recovery from synthetic wastewater using MFCs, experiments were carried out with actual industrial wastewater. Table 2 shows the composition of the industrial samples compared to the synthetic samples used in Section 3.2. While most of the properties remained comparable, the industrial samples contained extra cations such as $Ca^{2+}$ and $Mg^{2+}$, which might affect the removal efficiency by keeping the conductivity value constant in the wastewater (Lu et al., 2015).

Fig. 6 illustrates the electrochemical and $Zn^{2+}$ removal profiles during the treatment of industrial samples *A* and *B*. Similar trends were observed compared with the treatment of synthetic wastewater. The cathode potential decreased from +0.2 V to −0.2 V when the minimum operating potential of the bioanodes was reached (Fig. 6(a)) (Dominguez-Benetton et al., 2018; Nancharaiah et al., 2015). A current density of 0.10 ± 0.05 A/$m^2$ was measured, indicating the flow of electrons from the anode to the cathode (Fig. 6(b)). The current density in this experiment was slightly lower than that measured during experiments using synthetic wastewater (0.15 ± 0.05 A/$m^2$), which can be explained by the lower conductivity of industrial wastewater samples, in which no supporting electrolyte was added, compared with synthetic wastewater (2.3 & 1.7 mS/cm vs. 5.9 mS/cm, respectively) (Table 2). Despite the lower conductivity and current densities, the trend of $Zn^{2+}$ removal in the industrial samples was similar to that observed in the synthetic samples, with less than 3% (0.03 mM) $Zn^{2+}$ remaining at the end of the experiment (Fig. 6 (c)). The results provided evidence that the MFC is a suitable technology to treat these types of industrial samples regardless of their matrix complexity. The removal rates from the synthetic sample and industrial *Samples A* and *B* were 6.0, 7.3 and 12.2 mmol/$m^2$ cathode/h, respectively. As the level of the synthetic sample is less complex, the removal rate is the lowest compared to *Samples A* and *B*. Metal ion behaviour plays an important role in improving or deteriorating the performance of BESs (Lu et al., 2015). In this study, the alkali and alkaline earth metal ions present in the samples could have affected the MFC performance with a slight improvement in $Zn^{2+}$ removal. The improvement is attributed to the ionic strength and contribution of the conductivity of other anions to the catholyte. Solution conductivity is important to MFCs or bioelectrochemical systems (Karthikeyan et al., 2016). The experimental setup and the result in Section Fig. S1 confirmed the importance of the ionic strength and conductivity value (NaCl 3.0 g/L, 5.7 mS/cm vs. PBS 50 mM, 5.5 mS/cm). However, the ionic strength and conductivity value in actual wastewater were three orders of magnitude more diluted than those in the synthetic samples (refer Table 2). Other undetected species could have influenced the $Zn^{2+}$ removal process. Besides, organic matters such as acetate, if presented in the samples, can acted as ligands reacting with $Zn^{2+}$ to form metal complex and precipitated when the electrolyte pH was increased. Another possible explanation is the formation of metal oxides on the electrode surface acting as catalysts to reduce $O_2$ to $OH^-$. As shown in Fig. 6(c), the catholyte pH increased constantly from 7.8 to 8.4 for Sample A after 4 h and from 7.5 to 8.2 for Sample B after 3 h. This might also be due to the effect of the depleted $Zn^{2+}$ that

is available to couple with the hydroxides. However, soluble $Zn^{2+}$ may also deposit on the cathode surface as ZnO and act as an $O_2$ reduction catalyst to promote further $OH^-$ formation. It is well known that transition metal oxides are good catalyst materials for $O_2$ reduction (e.g., manganese (Roche and Scott, 2010), zinc (Yu et al., 2018), iron (Burkitt et al., 2016), cobalt (Zhao et al., 2019), etc.) and their performances can be further strengthened by coupling with other supported materials (e.g., graphene oxide (Yu et al., 2018), phthalocyanine (Burkitt et al., 2016), carbon nanotubes (Zhao et al., 2019), etc.). Meanwhile, the removal rate of *Sample B* is higher than that of *Sample A*, which can be attributed to their different initial concentrations of $Zn^{2+}$.

Fig. 7 represents the $Zn^{2+}$ removal efficiency and recovery from industrial samples. The results are consistent with the results using synthetic samples under the same conditions (batch mode, see Fig. 4). Approximately 97% of $Zn^{2+}$ was removed within 22 h for both industrial samples with different initial $Zn^{2+}$ concentrations. However, there is a large difference between the $Zn^{2+}$ electroprecipitated at the surface of the cathode and $Zn^{2+}$ precipitated in the medium. Nearly 58% less $Zn^{2+}$ was recovered from the cathode than from the catholyte. The complexity of industrial wastewaters (containing other cation species, as shown in Table 2) might affect the precipitation of zinc rather than its deposition onto the cathode surface. It is likely that other cation species

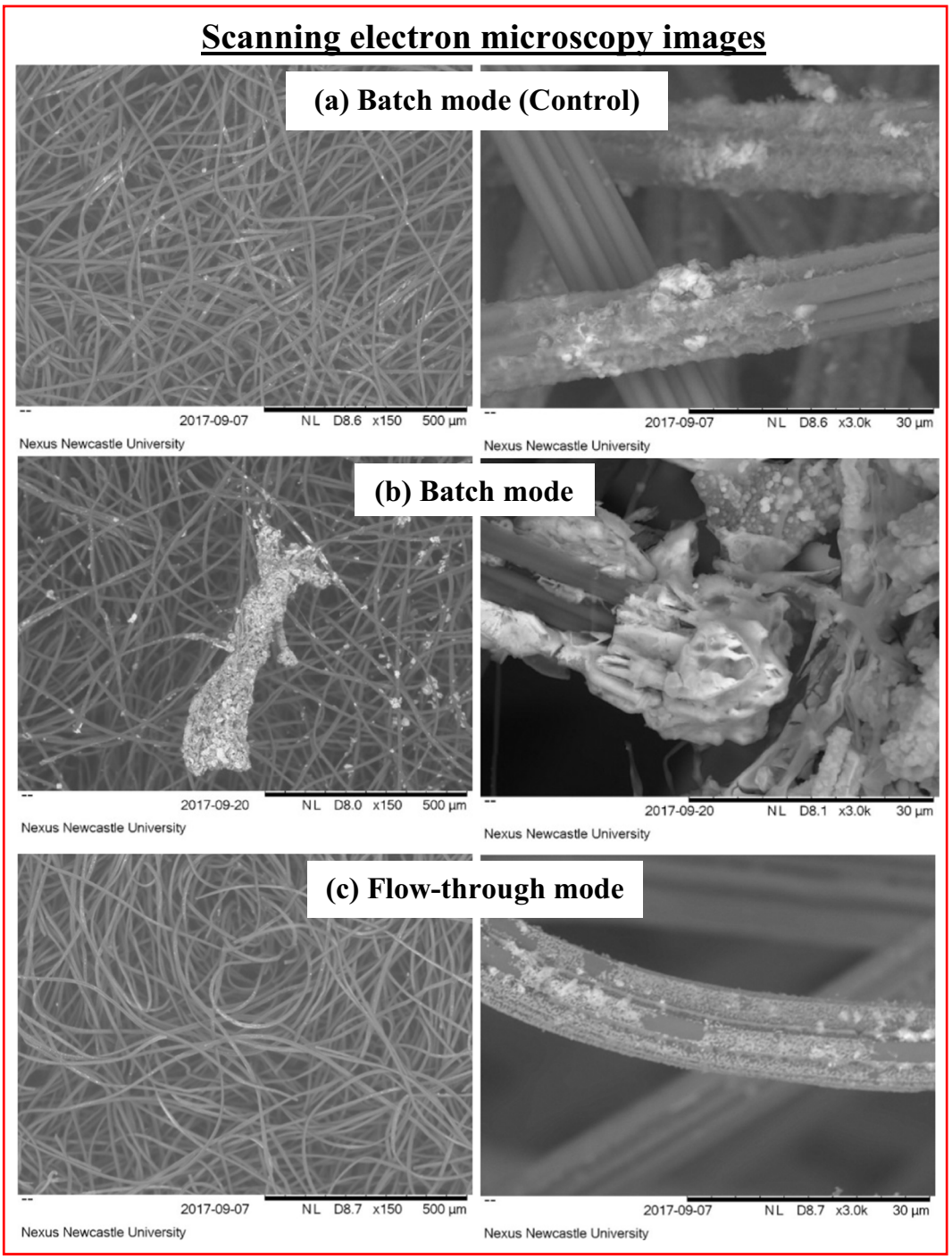


**Fig. 5.** Cathode surface morphology (analysed under SEM and EDX) after the zinc recovery process using synthetic wastewater under (a) control (open circuit condition), (b) batch mode anode, and (c) flow-through mode anode conditions.

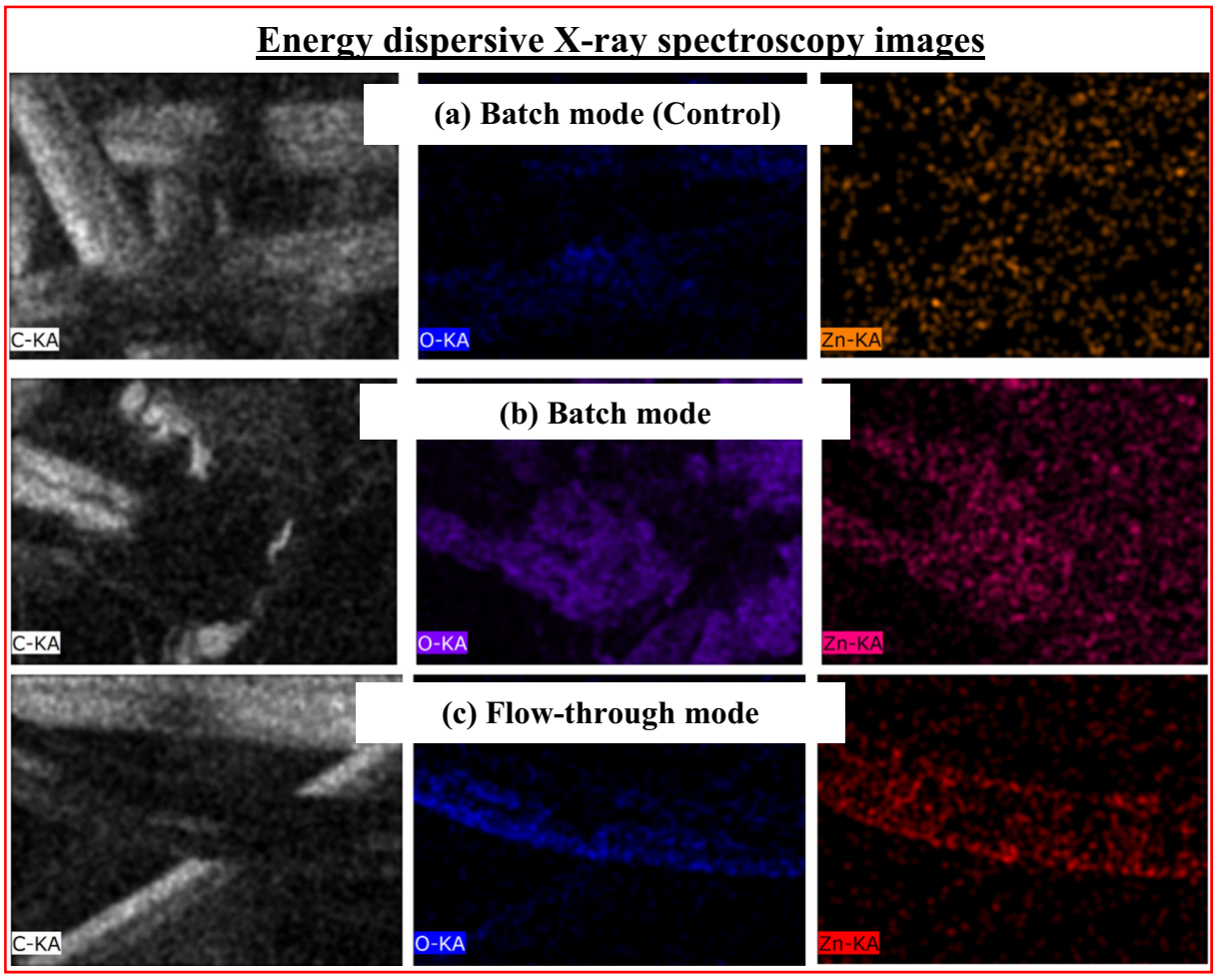


**Fig. 5** (*continued*).

(e.g., $Ca^{2+}$, $Pb^{2+}$) competed with $Zn^{2+}$ for electrons, inhibiting zinc reduction and precipitation activities on the cathode surface.

To achieve further Zn recovery, the collected $Zn(OH)_2$ would be re-dissolved in an acidic solution to obtain higher concentration. The high concentration Zn solution could be used for various applications directly or could further using electrodeposition to recover Zn metal. With higher concentration of Zn solution, the energy required would be lower. One of the examples is the well-known sulfuric acid leaching-electrowinning and the imperial smelting process used to treat the crude zinc oxide. For $Zn(OH)_2$ in MFC, it is a spontaneous reaction, therefore, no external energy required. The electrons produced from organic oxidation at the bioanode, were provided directly to cathode for ORR generating $OH^-$. For reducing $Zn^{2+}$ to Zn metal, the reduction potential $E°'^{2+}_{Zn/Zn} = -0.76$ V vs. SHE, which requires high energy input, $\Delta G = -2FE_{Zn/Zn2+}$. Also, in aqueous solution, water reduction with hydrogen evolution E = 0 V is competing with $Zn^{2+}$ for electrons. Electrons are more likely used by HER due to lower energy requirement, thus the efficiency for $Zn^{2+}$ reduction would be very low.

Fig. 8 presents the SEM/EDX images of cathodes after the removal of $Zn^{2+}$ from industrial samples. A layer of crystallised precipitates was noticed on the cathode surface, as shown in the SEM images (left side). In the second magnified SEM image (right side), thicker layers were found in the 10 Ω load-operated cathodes. A coagulated and crystallised structure was observed on *Sample B*, as the sample contained other classes of metal elements (Table 2), which may

**Table 2**
Properties and cation contents of synthetic and industrial samples.

| Metal ion classification[a] | | | Alkali metal | Alkaline earth metal | | Transition metal | Post-transition metal | Metalloid |
|---|---|---|---|---|---|---|---|---|
| Sample | pH | Conductivity | $[Na^+]$ | $[Mg^{2+}]$ | $[Ca^{2+}]$ | $[Zn^{2+}]$ | $[Pb^{2+}]$ | $[Si^{4+}]$ |
| | | mS/cm | mM | mM | mM | mM | mM | mM |
| Synthetic | 6.8 | 5.9 | 130.5[b] | – | – | 1.9 | – | – |
| Sample A | 6.7 | 2.3 | 0.4 | 1.3 | 2.0 | 1.2 | 0.002 | 0.046 |
| Sample B | 6.2 | 1.7 | 0.5 | 1.4 | 2.1 | 1.9 | 0.001 | 0.046 |

[a] According to Lu et al. (Lu et al., 2015), metal ion characteristics play an important role in improving or degrading the performance of BESs. They can directly influence electrolyte conductivity based on their position in the periodic table.
[b] NaCl (3.0 g/L) was added as a background agent to increase the solution conductivity.

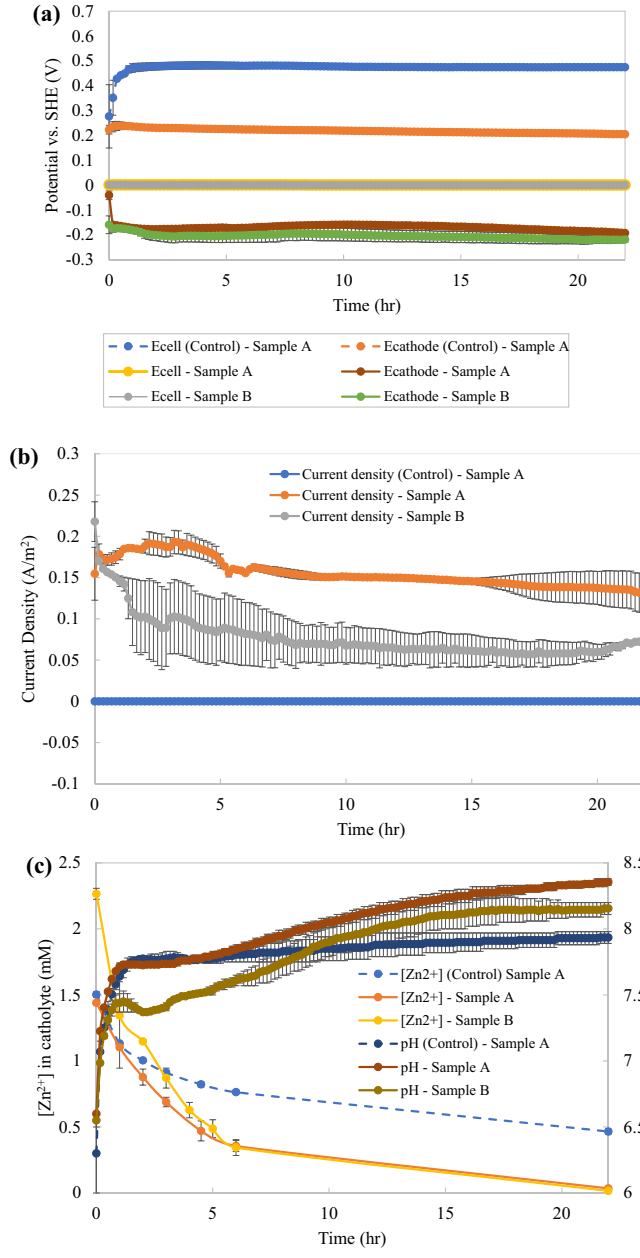


**Fig. 6.** Zinc recovery in MFCs from actual industrial wastewaters: (a) cell and electrode potentials, (b) current density, and (c) $Zn^{2+}$ concentration and catholyte pH. Note: Control: MFC operated under open circuit conditions; 10 Ω: MFC operated with a 10 Ω load resistor.

promote the formation of larger complexes. In addition to the crystallisation thickness, EDX results show higher signal intensities of the elements C, O and Zn on the cathode surface compared to the control (only *Sample A* control is shown). The colour intensity in the EDX results was stronger when the cathodes were operated under a load resistor. A thicker layer of $Zn(OH)_2$ was formed and crystallised due to the higher local pH and lower cathode potential favouring the production of $OH^-$ and the further deposition of $Zn(OH)_2$. In comparison to the synthetic sample, a mixed layer of $Zn(OH)_2$ with different colour intensities could be observed from the SEM result (obvious on the Sample B cathode surface). The distinct colour intensity might be due to the deposition of elements other than zinc, as mentioned in Table 2. The presence of these elements might also be the reason the deposition structure changed from dendritic (synthetic samples) to spherical (industrial samples).

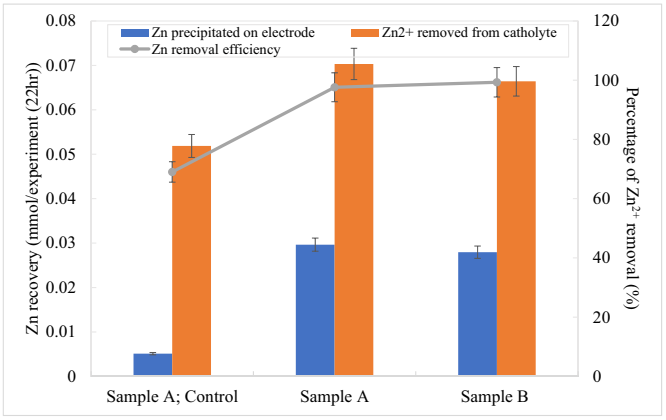


**Fig. 7.** Zinc recovery from the cathode, total removal from the catholyte and the removal efficiency in MFCs using actual wastewater.

### *3.4. Theoretical considerations and mathematical models for the removal of $Zn^{2+}$ using bioelectrochemical systems*

#### *3.4.1. Prediction of $Zn^{2+}$ removal feasibility using a Pourbaix diagram and standard reduction potential*

The standard reduction potential of the $Zn/Zn^{2+}$ couple is −0.76 V vs. SHE and can be written as:

$$Zn^{2+}(aq) + 2e^- \rightleftharpoons Zn\ (s)\quad E^{\circ\prime} = -0.76V\ \text{vs.SHE} \qquad \text{Reaction 1}$$

Considering the very negative potential of the $Zn/Zn^{2+}$ couple, a standalone MFC is unable to spontaneously achieve this reaction, i.e., without the assistance of any external power supply. Nevertheless, according to the Pourbaix diagram presented in Fig. 9 (reconstructed based on (Anonymous, n.d.; McMahon et al., 2019)), soluble $Zn^{2+}$ could be precipitated as $Zn(OH)_2$ under slightly alkaline pH conditions. As $Zn(OH)_2$ is insoluble in water, it gives an MFC-based system the advantage of removing $Zn^{2+}$ from wastewater by increasing the catholyte pH. Increasing the pH of the catholyte slightly above 7.0 is achievable by oxygen reduction under aerobic conditions. Based on the Pourbaix diagram, spontaneous $Zn(OH)_2$ precipitation can be achieved for $Zn^{2+}$ concentrations over 1 mM (65 ppm) as long as the solution pH is greater than 7.0; however, an alternative way of increasing the pH value is required for $Zn^{2+}$ concentrations below 1 mM (65 ppm). The prediction of spontaneous $Zn^{2+}$ removal by MFC (i.e., without the assistance of an external power supply) is marked in the blue region in Fig. 9. Two successive reactions are predicted: Reaction 2 is the oxygen reduction reaction under aerobic conditions leading to an increase in the local pH, and Reaction 3 is the subsequent zinc precipitation during which $Zn^{2+}$ in bulk reacts with $OH^-$ formed at the cathode surface:

$$O_2\ (g) + 2H_2O\ (l) + 4e^- \rightleftharpoons 4OH^-(aq)\quad E^{\circ\prime} = +0.40\ \text{V vs.SHE} \qquad \text{Reaction 2}$$

$$Zn^{2+}(aq) + 2OH^-(aq) \rightleftharpoons Zn(OH)_2(s) \qquad \text{Reaction 3}$$

The orange region depicted in Fig. 9 represents the area in which an MEC-based system (i.e., with the assistance of an external power supply) could be used for the direct recovery of metallic Zn from $Zn^{2+}$ (Reaction 1) or $Zn(OH)_2$ (Reaction 4). In such a system, the cathode potential would thus be much lower than −0.2 V. Indeed, the electrodeposition of metallic Zn would require a potential close to −1.0 V (or lower depending on pH and $Zn^{2+}$ concentration), at which the

hydrogen evolution reaction (HER) would be a significant side reaction, probably limiting the overall efficiency of the process.

$$Zn(OH)_2(s) + 2e^- \rightleftharpoons Zn(s) + 2OH^-(aq) \quad E^{\circ\prime} = -1.25\ V\ vs.SHE$$

Reaction 4

*3.4.2. Prediction of the equilibrium potential using the Nernst equation*

The Nernst equation was used to determine the specific potential at equilibrium other than the standard state (Renslow et al., 2011). It is written as:

$$E = E^{\circ\prime} - \frac{RT}{zF}\ \ln Q \quad (1)$$

where E is the reduction potential (V) at the temperature and concentration of interest, E°′ is the standard reduction potential (V), R is the universal constant ($R = 8.314\ J/(K\ mol)$), T is the temperature (K), z is the number of electrons transferred in the reaction, F is the Faraday constant (F = 96,485C/mol), and Q is the quotient of the reaction. The value Q is defined as:

$$Q = \frac{[Products]}{[Reactants]} \quad (2)$$

where [Products] is the total concentration of reductants and [Reactants] is the total concentration of oxidants. Therefore, the equilibrium

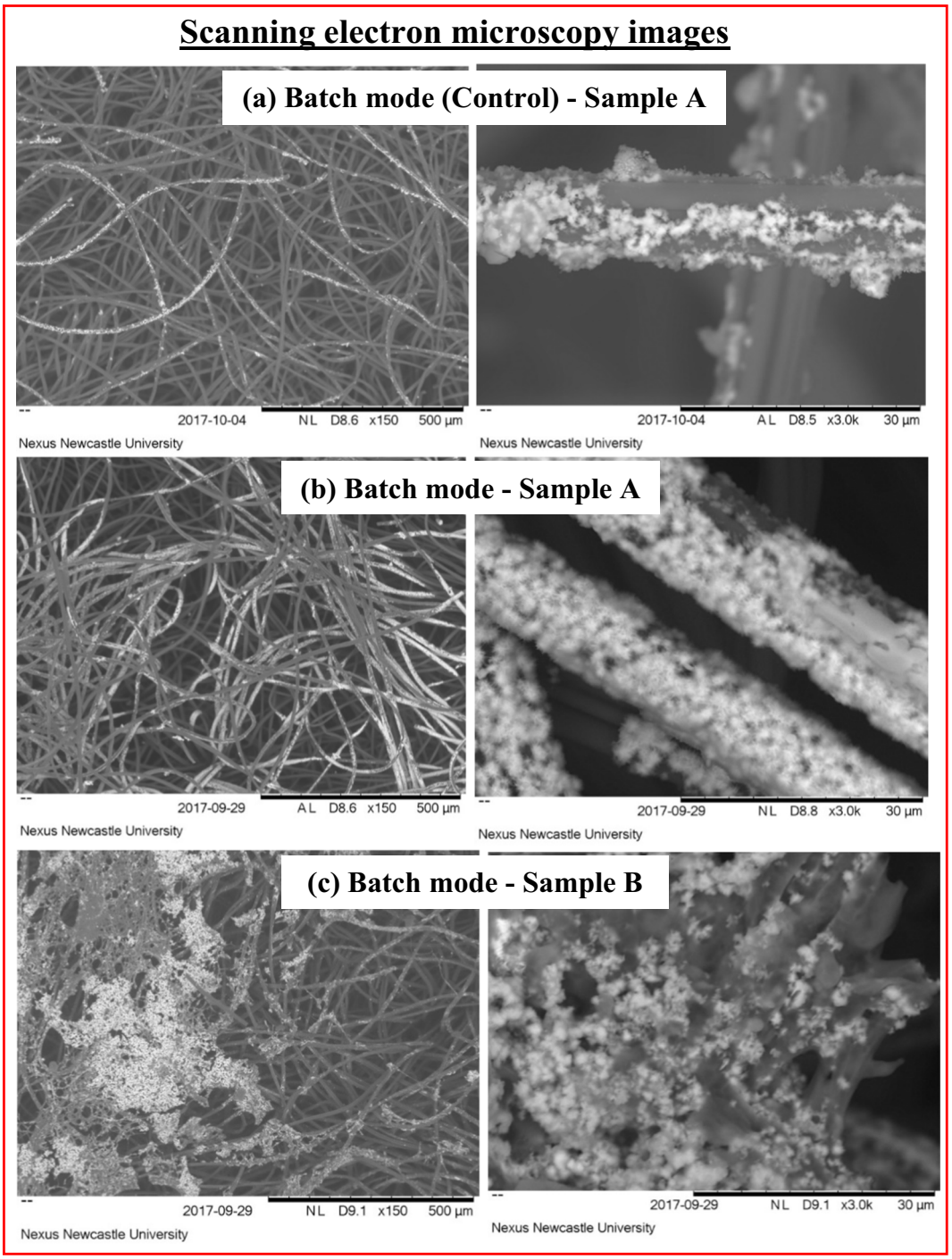


**Fig. 8.** Cathode surface morphology (analysed under SEM and EDX) after the zinc recovery process using industrial wastewaters under (a) control (open circuit condition), (b) batch mode anode - sample A and (c) batch mode anode - sample B conditions.

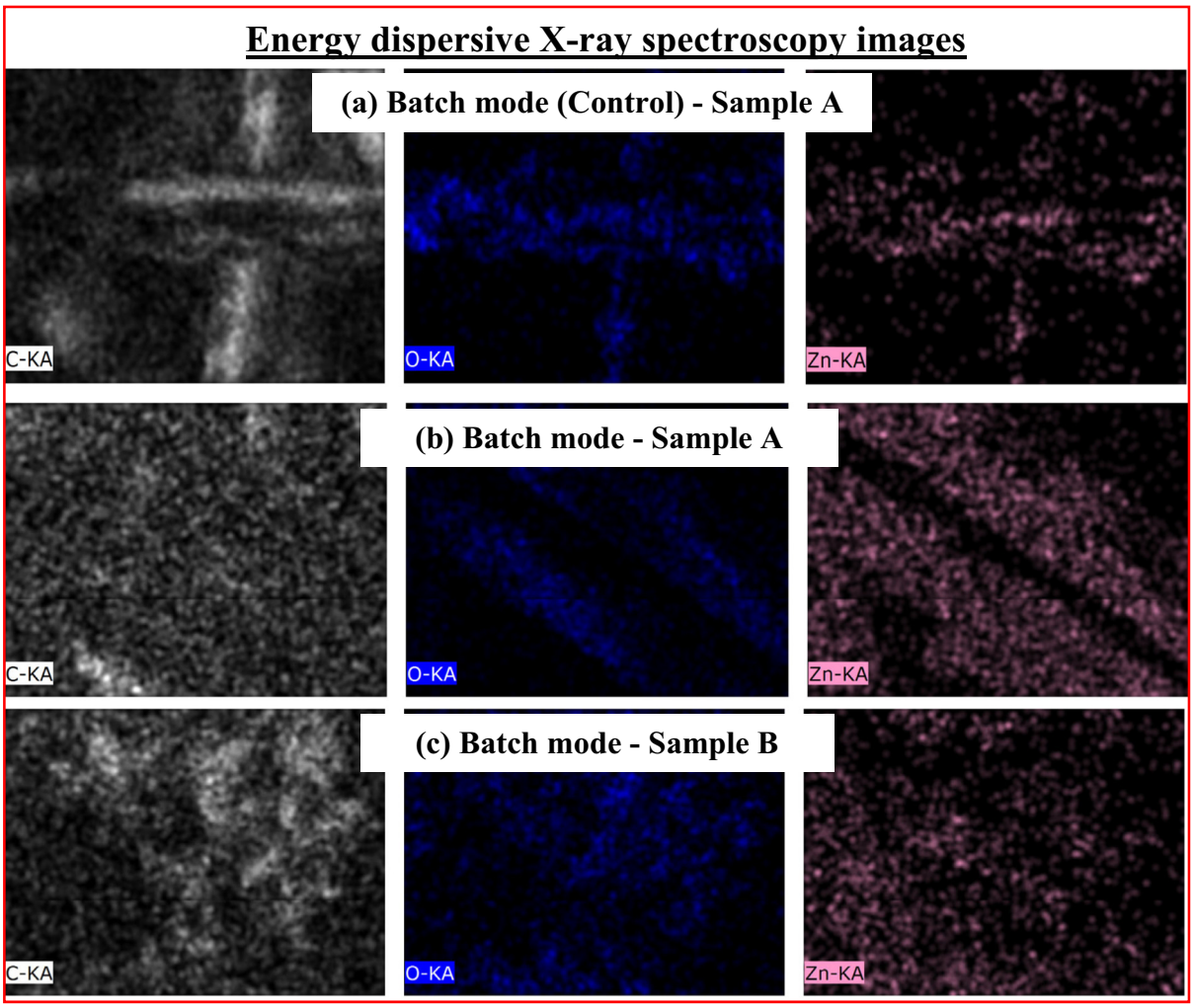


**Fig. 8** (*continued*).

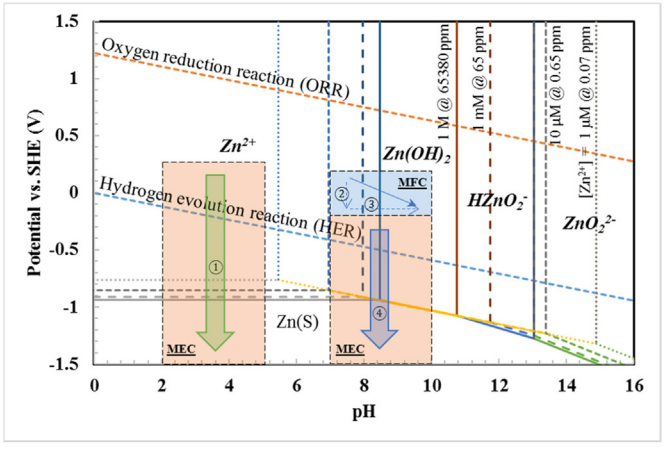


**Fig. 9.** Prediction of zinc removal from water based on Zn-water Pourbaix diagram in different $Zn^{2+}$ concentrations. The highlighted regions and arrows are possible $Zn^{2+}$ precipitation pathways (in a microbial fuel cell (MFC): Pathways ② & ③) or reduction pathways (in a microbial electrolysis cell (MEC): Pathways ① or ④) by using the cathode deposition technique assisted by external power. Note: Pathway ②: Low potential causes $O_2$ reduction and pH increase in solution. Pathway ③: Alkaline condition facilitates precipitation and deposition of $Zn^{2+}$ as $Zn(OH)_2$ on cathode surface. Pathways ① (acidic condition) and ④ (alkaline condition) require external power supply to assist metallic Zn reduction but hydrogen evolution reactions might take place as the applied potential is below the reaction line.

potential in this study, either a half-cell (anode or cathode) or complete cell can be predicted as in Table 3. The derived Nernst equations shown in the table are used to represent the direct (metallic) reduction of $Zn^{2+}$ (on the cathode side; Reaction 1), oxygen reduction reaction (on the cathode side; Reaction 2), acetate oxidation (on the anode side, Reaction 5) and complete reaction (combination of both anode and cathode; Reactions 2 and 5). The $[Zn^{2+}]$ and pH are the only parameters affecting the equilibrium potentials in Reaction 1 and Reaction 2, respectively. However, more than one compound was involved in Reaction 5, or Reactions 2 and 5, which required measurements of the organic (acetate) and inorganic carbon (carbonate) contents in the anolyte.

Fig. 10 presents the equilibrium potentials with respect to $[Zn^{2+}]$ under standard conditions (25 °C) and in experiments. In Fig. 10(a), the equilibrium potential was increased exponentially from −0.92 to −0.85 V vs. SHE when $[Zn^{2+}]$ was raised from 0 to 2.0 mM and reached a plateau after $[Zn^{2+}]$ was more than 2.0 mM. With respect to the temperature variations, the percentage of the potential difference was less than ±2% when the temperature was changed from the original 25 °C to ±25 °C. In Fig. 10(b), the experimental data were compared to the equilibrium potentials. According to the calculation, both potentials provided in the control and MFC modes were higher than the equilibrium potential of $[Zn^{2+}]$ in the solution. In the control, the cathode potential was +0.3 V vs. SHE and at least 1.1 V external potential ($\Delta E_1$) was required to bring the potential down to −0.8 V vs. SHE. In MFC mode, the potential gap was much smaller as the cathode potential was reduced from +0.3 V to 0 V vs. SHE; however, the driving force

**Table 3**
Summary of derived Nernst equations for the prediction of the oxidation, reduction, and cell potentials in a microbial fuel cell.

| Reaction | Formula | $E^{\circ\prime}$ (V vs. SHE) | Nernst equation | Note |
|---|---|---|---|---|
| 1 | $Zn\ (s) \rightleftharpoons Zn^{2+}\ (aq) + 2e^-$ | −0.76 | $E_{Zn^{2+}} = -0.76 - \frac{RT}{2F} \ln \frac{1}{[Zn^{2+}]}$ | Half-cell reduction reaction (cathode). |
| 2 | $O_2\ (g) + 2H_2O\ (l) + 4e^- \rightleftharpoons 4OH^-\ (aq)$ | +0.40 | $E_{OH^-} = 0.40 - \frac{2.303RT}{4F}(pH - 13.2756)$ | Half-cell reduction reaction (cathode): saturated $O_2$ (8.3 ppm) is assumed, pH + pOH = 14. |
| 5 | $CH_3COOH\ (aq) + 2H_2O\ (l) \rightleftharpoons 2CO_2\ (g) + 8H^+\ (aq) + 8e^-$ | −0.28 | $E_{CH_3COOH} = -0.28 - \frac{2.303RT}{8F}(\log \frac{[CO_2]}{CH_3COOH} - pH)$ | Half-cell oxidation reaction (bioanode): undetermined due to unknown acetate and $CO_2$ concentrations. |
| 2 + 5 | $CH_3COOH\ (aq) + 2O_2\ (g) \rightleftharpoons 2H_2O\ (l) + 2CO_2\ (g)$ | +0.68 | $E_{overall} = +0.68 - \frac{2.303RT}{8F}(\log \frac{[CO_2]}{[CH_3COOH]} - 0.7244)$ | Cell reaction (bioanode & cathode): undetermined due to unknown acetate and $CO_2$ concentrations. |

potential is still insufficient to drive metallic $Zn^{2+}$ reduction at −0.8 V vs. SHE and at least 0.8 V external power ($\Delta E_2$) was required. Modin et al. (Modin et al., 2012) showed in their results that the addition of diluted metals in the solution can change the cathode potential in response to the change in balance in chemical species under new steady-state conditions. Their cathode potential with added 4.59 mM $Zn^{2+}$ was recorded to be slightly higher (~0.05 V) compared to the control.

Fig. 11 depicts the comparison of the potential between $O_2/OH^-$ equilibrium and MFC-driven potentials. $Zn^{2+}$ can react with $OH^-$ to form insoluble compounds depending on the pH condition. MFC was used as an $OH^-$ production device (instead of direct reduction of $Zn^{2+}$, as mentioned above) to increase the pH in the catholyte via ORR. $O_2$ was continuously supplied by sparging air into the catholyte. The reducing power of the bioanode (0 V vs. SHE) was provided (channelled via an external circuit) to reduce the oxygen to hydroxide in the cathode according to Reaction 2. In Fig. 11(a), the ORR occurred faster in MFC mode than in the control. This is because the MFC cathode was assisted by the bioanode in reducing its reduction potential. Higher potential differential ($\Delta E_2 = 0.6$ V) was observed in MFC mode compared to the control ($\Delta E_1 = 0.2$ V). Even though the control was not assisted by the bioanode, a spontaneous reaction could occur due to ion complexity (where the Zn content is a function of pH and NaCl (McMahon et al., 2019)), chemical solubility (where the soluble $O_2$ is a function of partial pressure and air flow rate (Milner and Yu, 2018)), and environmental

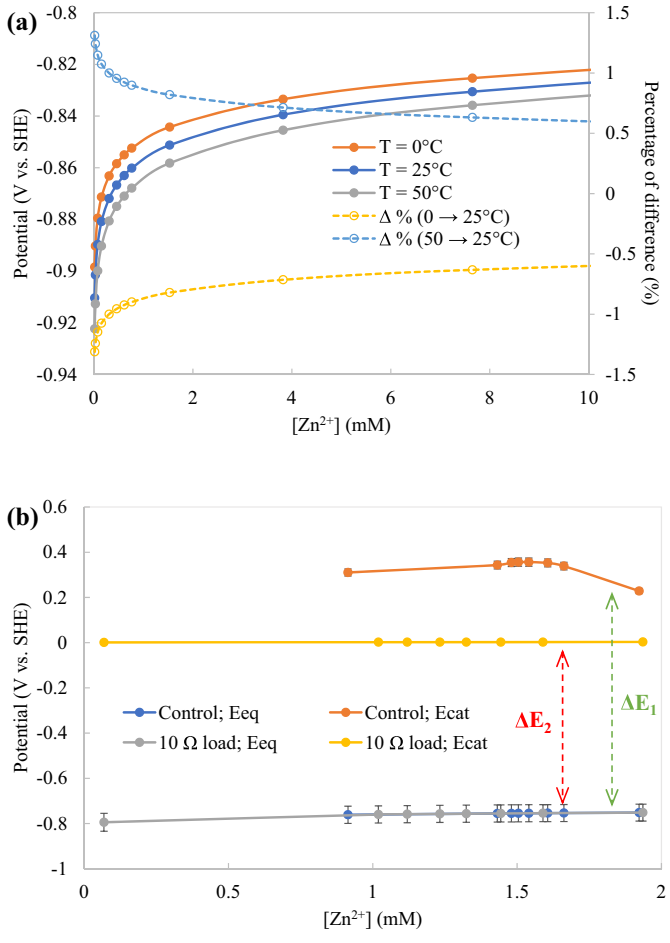


**Fig. 10.** (a) Estimation of the standard $Zn^{2+}$ reduction potential based on $Zn^{2+}$ concentration and temperature variation and (b) potential differential between the standard $Zn^{2+}$ reduction and MFC-driven potentials using the Nernst equation (Reaction 1). Note: $\Delta E_1$ (Control vs. Equilibrium) and $\Delta E_2$ (MFC vs. Equilibrium) indicate the potential differential of the experimental data from the estimation.

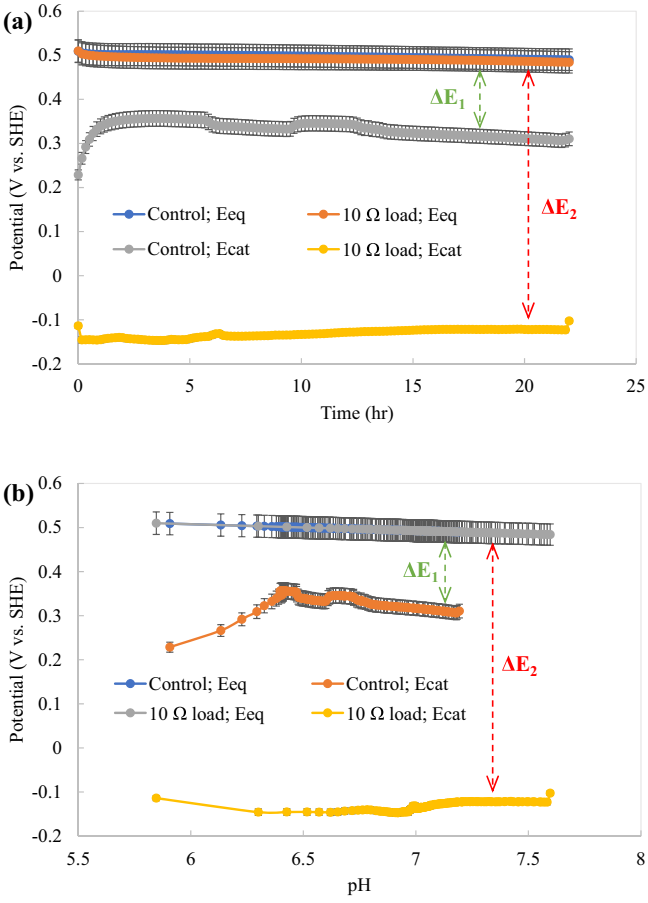


**Fig. 11.** Comparison of the equilibrium and MFC-driven potentials based on (a) time, and (b) pH. Note: $\Delta E_1$ (control vs. equilibrium) and $\Delta E_2$ (MFC-driven vs. equilibrium) indicate the potential differential of the experimental data from the Nernst equation (Reaction 2).

conditions (such as surface charge on the new electrode (Tombácz, 2009)). Similar potential differentials were observed under the pH changes in Fig. 11(b). Increases in pH could affect the $[Zn^{2+}]/[Zn(OH)_2]$ equilibrium to a specific condition where the cathode potential would favour the slow depletion of $[Zn^{2+}]$ over time (see Section 3.2).

*3.4.3. Prediction of removal time based on initial concentrations and applied current (the law of rate reaction)*

To facilitate the estimation of $Zn^{2+}$ removal, a rate law expression was used to explain the change in $Zn^{2+}$ over time. The reaction rates were derived according to the depletion of the $Zn^{2+}$ concentration in the treated solution (catholyte) over time. Reaction 1, Reaction 2, Reaction 3 or a combination of those reactions were used to derive the reaction rates in the previous sections [Section 3.1: metallic $Zn^{2+}$ reduction – external power input mode, Sections 3.2 & 3.3: Zinc precipitation via oxygen reduction reaction – MFC mode, and slow spontaneous removal – Control mode)]. The reaction rates are summarised as in For Reaction 2, $O_2$ reduction is assumed to occur via a single-step reaction. The reaction process is simplified, as the actual mechanism involves several intermediate steps during the transition from $O_2$ to $OH^-$, including the possible formation of hydrogen peroxide (Milner et al., 2017; Wu et al., 2011; Nørskov et al., 2004). Table 4. For Reaction 2, $O_2$ reduction is assumed to occur via a single-step reaction. The reaction process is simplified, as the actual mechanism involves several intermediate steps during the transition from $O_2$ to $OH^-$, including the possible formation of hydrogen peroxide (Milner et al., 2017; Wu et al., 2011; Nørskov et al., 2004).

According to Faraday's law of electrolysis, the applied current over the time of $Zn^{2+}$ removal can be expressed as:

$$I_D A_c = \frac{nzF}{t} = \frac{\left(\left[Zn^{2+}\right]^{\circ} - \left[Zn^{2+}\right]\right) V_c zF}{t} \quad (3)$$

where $I_D$ is the current density ($A/m^2$), $A_c$ is the cathode projected area ($0.03^2$ $m^2$), n is the amount of the deposited/reduced Zn (mol) equal to $([Zn^{2+}]^{\circ}\text{-}[Zn^{2+}])V_c$, $[Zn^{2+}]^{\circ}$ is the initial $Zn^{2+}$ concentration (M), $[Zn^{2+}]$ is the $Zn^{2+}$ concentration at time t (M), $V_c$ is the catholyte volume ($0.0001$ $m^3$), z is the number of electrons transferred, which is 2 in the reaction, F is the Faraday constant (F = 96,485C/mol), and t is the time (s). Rearranged into linear form (y = mx + c), the $Zn^{2+}$ concentration, $[Zn^{2+}]$ at a specific electrolysis time, t is written as:

$$\left[Zn^{2+}\right] = -\frac{I_D A_c}{zFV_c} t + \left[Zn^{2+}\right]^{\circ} \quad (4)$$

By comparing with the rate equation in For Reaction 2, $O_2$ reduction is assumed to occur via a single-step reaction. The reaction process is simplified, as the actual mechanism involves several intermediate steps during the transition from $O_2$ to $OH^-$, including the possible formation of hydrogen peroxide (Milner et al., 2017; Wu et al., 2011; Nørskov et al., 2004). Table 4: Reaction 1, $I_D A_c/zF$ is equal to the zero-order reaction coefficient, k. If all $Zn^{2+}$ in the solution was removed, $[Zn^{2+}] = 0$ and the maximum time of removal, $t_{max}$ can be estimated as:

$$t_{max} = \frac{\left[Zn^{2+}\right]^{\circ} zFV_c}{I_D A_c} \quad (5)$$

Table 5 shows the values of the reaction coefficient, k and initial $Zn^{2+}$ concentration. Most of the fitted data showed a high value of fitting, $R^2$ (>0.99), except for the abiotic cell test under applied currents of 0 and 0.06 $A/m^2$. Table 5 (1) summarises all coefficient values determined from the abiotic cell tests using a zero-order reaction model. The rate law equation is not meant to be used for zero applied current as no reaction occurred or the reaction was driven by the fixed current. $Zn^{2+}$ removal barely occurred at 0.06 $A/m^2$ fixed current. This is because the direct reduction of $Zn^{2+}$ to metallic Zn requires at least −0.76 V vs. SHE. It is believed that the cathodic potential was still higher than the standard reduction potential to perform an effective reduction reaction. From the results shown in Fig. 2, it could be observed that the pH and $Zn^{2+}$ concentration was maintained even though the cell potential was increased from −0.50 to 0.85 V (the cathode potential was not recorded) when the applied current was set from 0 to 0.06 $A/m^2$. In the abiotic cell test, the reaction coefficient k increased (0.040 to 1.342 mM/h), while the reaction half-life $t_{1/2}$ decreased (22.643 to 0.724 h) as the fixed current $I_D$ increased from 0.06 to 5.56 $A/m^2$ with the initial $Zn^{2+}$ concentration, $[Zn^{2+}]^{\circ}$ equalled 1.99 ± 0.18 mM. A similar trend is also noticeable in the MFC mode and control, where k was disproportional with $t_{1/2}$.

**Table 4**
Mathematical estimation of the reaction rate and assumptions for the removal of $Zn^{2+}$ in abiotic cells, MFCs, and control modes.

| Reaction | Formula | $E^{\circ\prime}$ (V vs. SHE) | Original rate expression | Reaction rate & half-life reaction | Note |
|---|---|---|---|---|---|
| 1 | $Zn\ (s) \rightleftharpoons Zn^{2+}\ (aq) + 2e^-$ | −0.76 | $r^a = k\,[Zn^{2+}]$ | $r = k$<br>$t_{1/2} = [Zn^{2+}]/2\ k$<br>(*Zero order*)<br>**Linear equation**:<br>$[Zn^{2+}] = -kt + [Zn^{2+}]^{\circ}$<br>**Faraday equation**:<br>$[Zn^{2+}] = -(I_D A_c/zFV_c)\ t + [Zn^{2+}]^{\circ}$<br>$t_{max} = [Zn^{2+}]^{\circ} zFV_c/I_D A_c$ | **Abiotic cell mode**: in the direct (metallic) $Zn^{2+}$ reduction, $Zn^{2+}$ removal is depended on applied current (with the cathode potential ≤ −0.76 V vs. SHE). Therefore, the $[Zn^{2+}]$ is an independent parameter in the rate law equation which has no effect on the removal rate, r.<br>The rate coefficient, k is equal to $I_D A_c/zF$ (derived from Faraday's law of electrolysis (see Eq. (4)). |
| 3 | $Zn^{2+}\ (aq) + 2OH^-\ (aq) \rightleftharpoons Zn(OH)_2\ (s)$ | Not available | $r^a = k\,[Zn^{2+}]\,[OH^-]^2$ | $r = k\,[Zn^{2+}]$<br>$t_{1/2} = \ln 2/k$<br>(*First order*)<br>**Linear equation**:<br>$\ln [Zn^{2+}] = -kt + \ln [Zn^{2+}]^{\circ}$ | **MFC mode**: Zn removal depended on available $OH^-$ and the $OH^-$ is depended on the current provided by bioanode, indirectly limiting $Zn^{2+}$ removal. $[OH^-]$ is considered as an independent parameter due to continuous production (unlimited) of $OH^-$ under oxygen reduction reaction (as long as the bioanode keep supplying the electrons to cathode with unlimited supplied of $O_2$ by air purging). |
| 2 + 3 | $2Zn^{2+}\ (aq) + O_2\ (g) + 2H_2O\ (l) + 4e^- \rightleftharpoons 2Zn(OH)_2\ (s)$ | +0.40 | $r^a = k\,[Zn^{2+}]^2\,[O_2]\,[H_2O]^2$ | $r = k\,[Zn^{2+}]^2$<br>$t_{1/2} = 1/k\,[Zn^{2+}]$<br>(*Second order*)<br>**Linear equation**:<br>$1/[Zn^{2+}] = kt + 1/[Zn^{2+}]^{\circ}$ | **Control mode**: slow but spontaneous reaction as small amount of negative charge might be available at local environment where the reaction takes place. $[O_2]$ and $[H_2O]$ are independent parameters due to unlimited supplied by air sparging in aqueous environment. |

[a] All reactions are assumed to occur under standard conditions (1 atm, 25 °C).

**Table 5**
Summary of the reaction coefficient (k), initial concentration ($[Zn^{2+}]°$), and reaction half-life ($t_{1/2}$) values for (1) abiotic cell test, (2) MFC mode, and (3) control.

| (1) Abiotic cell test[a] | Reaction coefficient, k[d] | Initial concentration, $[Zn^{2+}]°$ | Reaction half-life, $t_{1/2}$ | $R^2$ |
|---|---|---|---|---|
| Fixed current, $I_D$ | | | | |
| $A/m^2$ | mM/h | mM | hr | |
| 0 | N.A. | N.A. | N.A. | N.A. |
| 0.06 | 0.040 | 1.817 | 22.64 | 0.017 |
| 0.22 | 0.119 | 2.037 | 8.57 | 0.797 |
| 0.56 | 0.163 | 1.964 | 6.02 | 0.964 |
| 2.22[e] | 0.658 | 2.176 | 1.66 | 0.997 |
| 5.56 | 1.342 | 1.944 | 0.72 | 0.734 |
| (2) MFC mode[b] | Reaction coefficient, k | Initial concentration, $[Zn^{2+}]°$ | Reaction half-life, $t_{1/2}$ | $R^2$ |
| 10 Ω load resistor | 1/h | mM | hr | |
| Batch | 0.099 | 1.822 | 6.97 | 0.975 |
| Flow-through | 0.059 | 1.790 | 11.70 | 0.936 |
| Sample A | 0.235 | 1.409 | 2.95 | 0.998 |
| Sample B | 0.296 | 2.066 | 2.34 | 0.988 |
| (3) Control[c] | Reaction coefficient, k | Initial concentration, $[Zn^{2+}]°$ | Reaction half-life, $t_{1/2}$ | $R^2$ |
| Open circuit | (1/mM)/hr | mM | hr | |
| Batch | 0.026 | 1.800 | 21.45 | 0.886 |
| Sample A | 0.102 | 1.338 | 7.33 | 0.948 |

[a] Zero-order reaction.
[b] First-order reaction.
[c] Second-order reaction.
[d] A linear relationship (k vs. $I_D$) can be plotted as $k = 0.236\ I_D + 0.0574$ where $k_o = 0.0574$ mM/h.
[e] Maximum current density that can be achieved in batch mode MFC (refer Fig. S1).

Tao et al. (Tao et al., 2014) conducted an experiment using a mixture of heavy metals (initial concentration) consisting of $Cu^{2+}$ (12.6), $Pb^{2+}$ (1.93), and $Zn^{2+}$ (7.12). The experiment treated $Cu^{2+}$ (under MFC mode) first followed by $Pb^{2+}$ and $Zn^{2+}$ (electrolysis) in sequential order corresponding to their standard reduction potentials. More than 90% removal was recorded for each metal element within 10 h of treatment. They found that the experimental data fit well using a first-order reaction model with reaction coefficients and k values (1/h) of 0.1603, 0.3620 and 0.3245 for $Cu^{2+}$, $Pb^{2+}$, and $Zn^{2+}$, respectively. In our study (see Table 5 (2)), the values of $Zn^{2+}$ removal were estimated at 0.235 and 0.296/h for industrial samples A and B, respectively. The slight difference in the values was due to the initial $Zn^{2+}$ concentration between the samples (A: 1.409 and B: 2.066 mM). Surprisingly, the k value was low using synthetic samples under the same experimental conditions. It was calculated as 0.099/h, which is half of the industrial sample values. The slow reaction rate in the synthetic sample (indicated by the k value) increased the half reaction time, $t_{1/2,}$ by more than two times (6.97 h) compared to the industrial samples (2.34–2.95 h). The flow-through mode had the lowest k (0.059/h) and highest $t_{1/2}$ (11.70 h) values, which were simply due to the ineffective operation of the bioanode in comparison with the batch mode. Table 5 (3) summarises the values of the coefficients in control (operated under open circuit conditions). It was found that the experimental data fit well using the second-order reaction model. Second-order reaction kinetics is represented in well-known models applied in heavy metal adsorption research to study the chemical sorption (chemisorption) properties on an active material surface. Literature reviews (Bankole et al., 2019b; Anoop Krishnan et al., 2016; Sharifpour et al., 2018a) have shown that activated carbon and its derivatives (e.g., carbon nanotubes and sulfurized carbon) are good materials for heavy metal adsorption and removal. New carbon felt was replaced for every experiment and could present the adsorption behaviours to remove $Zn^{2+}$ in solution under the control condition. This is due to the attraction of the valence force with electrons being shared between the heavy metal cations and the adsorbent (carbon felt in our case) (Sharifpour et al., 2018b). The k value recorded for industrial sample A was 0.102/(mM hr), which is higher than that of the synthetic sample (0.026/(mM hr)). Meanwhile, $t_{1/2}$ was 7.33 h for industrial sample A and 21.45 h for the synthetic sample. The $t_{1/2}$ values showed that $Zn^{2+}$ removal was possible under control conditions compared to the MFC mode; however, the removal rate was much slower, which also indicated the importance of the MFC bioanode in assisting the removal.

In this study, a self-sustaining MFC powered by a bioanode was used to support $Zn^{2+}$ removal from synthetic and industrial wastewater. Apart from the energy-saving advantage, the $Zn^{2+}$ removal efficiency (96%) was competitive in comparison to other similar studies (see Table 1) with a reasonable removal period (22h). The main process behind the removal is the increase in catholyte pH via the oxygen reduction reaction driven by the bioanode to assist the precipitation of $Zn(OH)_2$.

## 4. Conclusion

The study demonstrated the feasibility of MFCs for the removal of Zn from actual industrial wastewaters without the assistance of an external energy supply. The initial $Zn^{2+}$ concentration in the wastewater was determined to be $1.55 \pm 0.35$ mM. The removal efficiencies were between 96 and 99%. However, the zinc recovery in terms of $Zn(OH)_2$ accumulation on the cathode surface was 83 and 42% for the synthetic and industrial samples, respectively, while the rest of the zinc precipitate was found in the remaining catholyte. The low level of precipitation attachment on the cathode surface might be due to the complexity and conductivity of the wastewater. Unlike the direct reduction of $Zn^{2+}$ in electrolysis, $Zn(OH)_2$ is formed and agglomerates through weak intermolecular forces, tending to detach from the cathode surface during hydroxide precipitation. The prediction of $Zn^{2+}$ removal using models derived from the Nernst equation and rate law expressions was successfully achieved. The study showed that the bioanode was an important component in providing the required potential to drive equilibrium into a new steady state with less diluted $Zn^{2+}$. Finally, the removal performances in the electrolysis, MFC and control setup were determined using rate law expressions. The results showed that the decreases in

$Zn^{2+}$ concentration in electrolysis (direct reduction), MFC (indirect via $O_2$ reduction) and control (chemisorption) followed zero-, first- and second-order reaction rates, respectively. The reaction half-life, $t_{1/2,}$ of the MFCs was 6.97 h, which is longer than the electrolysis process recorded as 1.66 h as a result of the process receiving sufficient energy input to promote direct reduction of $Zn^{2+}$ to metallic Zn. Even though no external energy was provided in the cathode to assist $Zn^{2+}$ removal, the control recorded the longest reaction half-life, which was 21.45 h. The highest reaction half-life value could be related to the adsorption behaviour of the cathode, which slowly removed $Zn^{2+}$ from the solution. Overall, it was shown that no external electrical energy source or chemicals were required in the MFC mode process as the energy was supplied by the bioanode, showing that the MFC can operate as a standalone unit for the removal of $Zn^{2+}$ from industrial wastewater.

## CRediT authorship contribution statement

**Swee Su Lim:** Writing – original draft, Formal analysis, Validation. **Jean-Marie Fontmorin:** Writing – review & editing, Visualization. **Hai The Pham:** Investigation, Resources, Data curation. **Edward Milner:** Conceptualization, Methodology. **Peer Mohamed Abdul:** Validation. **Keith Scott:** Supervision. **Ian Head:** Supervision, Funding acquisition. **Eileen Hao Yu:** Supervision, Project administration.

## Declaration of competing interest

The authors declare that they have no known competing financial interests or personal relationships that could have appeared to influence the work reported in this paper.

## Acknowledgements

This research was financially supported by the Natural Environment Research Council [NE/L01422X/1]; the Engineering and Physical Sciences Research Council [EP/N009746/1]; National Biofilm Innovation Centre [01POC18047]; EPSRC Impact accelerate awards (IAA) and Universiti Kebangsaan Malaysia [GGPM-2019-028 & PP-SELFUEL-2020]. The authors also thank Chemviron Carbon Limited, Tipton, UK for providing real $Zn^{2+}$-containing wastewater samples. Further metadata to this article can be found online at 10.25405/data.ncl.14069135

## Appendix A. Supplementary data

Supplementary data to this article can be found online at https://doi.org/10.1016/j.scitotenv.2021.145934.

## References

Abourached, C., Catal, T., Liu, H., 2014. Efficacy of single-chamber microbial fuel cells for removal of cadmium and zinc with simultaneous electricity production. Water Res. 51, 228–233. https://doi.org/10.1016/j.watres.2013.10.062.

Anonymous, The Nernst Equation and Pourbaix diagram, (n.d.). https://www.doitpoms.ac.uk/tlplib/pourbaix/index.php (accessed June 16, 2020).

Anoop Krishnan, K., Sreejalekshmi, K.G., Vimexen, V., Dev, V.V., 2016. Evaluation of adsorption properties of sulphurised activated carbon for the effective and economically viable removal of Zn(II) from aqueous solutions. Ecotoxicol. Environ. Saf. 124, 418–425. https://doi.org/10.1016/j.ecoenv.2015.11.018.

Bankole, M.T., Abdulkareem, A.S., Mohammed, I.A., Ochigbo, S.S., Tijani, J.O., Abubakre, O.K., Roos, W.D., 2019a. Selected heavy metals removal from electroplating wastewater by purified and polyhydroxylbutyrate functionalized carbon nanotubes adsorbents. Sci. Rep. 9, 4475. https://doi.org/10.1038/s41598-018-37899-4.

Bankole, M.T., Abdulkareem, A.S., Mohammed, I.A., Ochigbo, S.S., Tijani, J.O., Abubakre, O.K., Roos, W.D., 2019b. Selected heavy metals removal from electroplating wastewater by purified and polyhydroxylbutyrate functionalized carbon nanotubes adsorbents. Sci. Rep. 9, 4475. https://doi.org/10.1038/s41598-018-37899-4.

Burkitt, R., Whiffen, T.R., Yu, E.H., 2016. Iron phthalocyanine and MnOx composite catalysts for microbial fuel cell applications. Appl. Catal. B Environ. 181, 279–288. https://doi.org/10.1016/j.apcatb.2015.07.010.

S.M. Daud, W.R.W. Daud, B.H. Kim, M.R. Somalu, M.H.A. Bakar, A. Muchtar, J.M. Jahim, S.S. Lim, I.S. Chang, Comparison of performance and ionic concentration gradient of two-chamber microbial fuel cell using ceramic membrane (CM) and cation exchange membrane (CEM) as separators, Electrochim. Acta. 259 (2018). doi:https://doi.org/10.1016/j.electacta.2017.10.118.

Dominguez-Benetton, X., Varia, J.C., Pozo, G., Modin, O., Ter Heijne, A., Fransaer, J., Rabaey, K., 2018. Metal recovery by microbial electro-metallurgy. Prog. Mater. Sci. 94, 435–461. https://doi.org/10.1016/j.pmatsci.2018.01.007.

C. Fang, V. Achal, The Potential of Microbial Fuel Cells for Remediation of Heavy Metals from Soil and Water—Review of Application, Microorganisms. 7 (2019). doi:https://doi.org/10.3390/microorganisms7120697.

Fradler, K.R., Michie, I., Dinsdale, R.M., Guwy, A.J., Premier, G.C., 2014. Augmenting microbial fuel cell power by coupling with supported liquid membrane permeation for zinc recovery. Water Res. 55, 115–125. https://doi.org/10.1016/j.watres.2014.02.026.

Fu, F., Wang, Q., 2011. Removal of heavy metal ions from wastewaters: a review. J. Environ. Manag. 92, 407–418. https://doi.org/10.1016/j.jenvman.2010.11.011.

Huang, L., Li, T., Liu, C., Quan, X., Chen, L., Wang, A., Chen, G., 2013. Synergetic interactions improve cobalt leaching from lithium cobalt oxide in microbial fuel cells. Bioresour. Technol. 128, 539–546. https://doi.org/10.1016/j.biortech.2012.11.011.

Karthikeyan, R., Selvam, A., Cheng, K.Y., Wong, J.W.-C., 2016. Influence of ionic conductivity in bioelectricity production from saline domestic sewage sludge in microbial fuel cells. Bioresour. Technol. 200, 845–852. https://doi.org/10.1016/j.biortech.2015.10.101.

Lee, C.-Y., Huang, Y.-N., 2013. The effects of electrode spacing on the performance of microbial fuel cells under different substrate concentrations. Water Sci. Technol. 68, 2028–2034. https://doi.org/10.2166/wst.2013.446.

Lefebvre, O., Neculita, C.M., Yue, X., Ng, H.Y., 2012. Bioelectrochemical treatment of acid mine drainage dominated with iron. J. Hazard. Mater. 241–242, 411–417. https://doi.org/10.1016/j.jhazmat.2012.09.062.

S.S. Lim, E.H. Yu, W.R.W. Daud, B.H. Kim, K. Scott, Bioanode as a limiting factor to biocathode performance in microbial electrolysis cells, Bioresour. Technol. 238 (2017). doi:https://doi.org/10.1016/j.biortech.2017.03.127.

Lu, Z., Chang, D., Ma, J., Huang, G., Cai, L., Zhang, L., 2015. Behavior of metal ions in bioelectrochemical systems: a review. J. Power Sources 275, 243–260. https://doi.org/10.1016/j.jpowsour.2014.10.168.

Luo, H., Qin, B., Liu, G., Zhang, R., Tang, Y., Hou, Y., 2015. Selective recovery of Cu2+ and Ni2+ from wastewater using bioelectrochemical system. Front. Environ. Sci. Eng. 9, 522–527. https://doi.org/10.1007/s11783-014-0633-5.

McMahon, M.E., Santucci, R.J., Scully, J.R., 2019. Advanced chemical stability diagrams to predict the formation of complex zinc compounds in a chloride environment. RSC Adv. 9, 19905–19916. https://doi.org/10.1039/C9RA00228F.

E.M. Milner, E.H. Yu, The Effect of Oxygen Mass Transfer on Aerobic Biocathode Performance, Biofilm Growth and Distribution in Microbial Fuel Cells, Fuel Cells. 18 (2018) 4–12. doi:doi:https://doi.org/10.1002/fuce.201700172.

Milner, E.M., Scott, K., Head, I.M., Curtis, T., Yu, E.H., 2017. Evaluation of porous carbon felt as an aerobic biocathode support in terms of hydrogen peroxide. J. Power Sources 356, 459–466. https://doi.org/10.1016/j.jpowsour.2017.03.079.

J.A. Modestra, G. Velvizhi, K.V. Krishna, K. Arunasri, P.N.L. Lens, Y. Nancharaiah, S.V. Mohan, E.R. Rene, E. Sahinkaya, A. Lewis, P.N.L. Lens, Bioelectrochemical systems for heavy metal removal and recovery, in: Sustain. Heavy Met. Remediat. vol. 1 Princ. Process., Springer, 2017: pp. 165–198. doi:https://doi.org/10.1007/978-3-319-58622-9_6.

Modin, O., Wang, X., Wu, X., Rauch, S., Fedje, K.K., 2012. Bioelectrochemical recovery of Cu, Pb, Cd, and Zn from dilute solutions. J. Hazard. Mater. 235–236, 291–297. https://doi.org/10.1016/j.jhazmat.2012.07.058.

Modin, O., Fuad, N., Rauch, S., 2017. Microbial electrochemical recovery of zinc. Electrochim. Acta 248, 58–63. https://doi.org/10.1016/j.electacta.2017.07.120.

Y. V Nancharaiah, S. Venkata Mohan, P.N.L. Lens, Metals removal and recovery in bioelectrochemical systems: A review, Bioresour. Technol. 195 (2015) 102–114. doi:https://doi.org/10.1016/j.biortech.2015.06.058.

Nørskov, J.K., Rossmeisl, J., Logadottir, A., Lindqvist, L., Kitchin, J.R., Bligaard, T., Jónsson, H., 2004. Origin of the overpotential for oxygen reduction at a fuel-cell cathode. J. Phys. Chem. B 108, 17886–17892. https://doi.org/10.1021/jp047349j.

Renslow, R., Donovan, C., Shim, M., Babauta, J., Nannapaneni, S., Schenk, J., Beyenal, H., 2011. Oxygen reduction kinetics on graphite cathodes in sediment microbial fuel cells. Phys. Chem. Chem. Phys. 13, 21573–21584. https://doi.org/10.1039/c1cp23200b.

Roche, I., Scott, K., 2010. Effect of pH and temperature on carbon-supported manganese oxide oxygen reduction electrocatalysts. J. Electroanal. Chem. 638, 280–286. https://doi.org/10.1016/j.jelechem.2009.10.030.

P. Rodenas Motos, A. ter Heijne, R. van der Weijden, M. Saakes, C.J.N. Buisman, T.H.J.A. Sleutels, High rate copper and energy recovery in microbial fuel cells, Front. Microbiol. 6 (2015). doi:https://doi.org/10.3389/fmicb.2015.00527.

S.E.P.A (SEPA), Scottish pollutant release inventory, (2018). http://apps.sepa.org.uk/spripa/Pages/SubstanceInformation.aspx?pid=111.

Sharifpour, E., Haddadi, H., Ghaedi, M., Dashtian, K., Asfaram, A., 2018a. Synthesis of antimicrobial cationic amphiphile functionalized mesocellular silica foam prepared on hard template/support activated carbon for enhanced simultaneous removal of Cu (II) and Zn(II) ions. J. Environ. Chem. Eng. 6, 4864–4877. https://doi.org/10.1016/j.jece.2018.07.029.

Sharifpour, E., Haddadi, H., Ghaedi, M., Dashtian, K., Asfaram, A., 2018b. Synthesis of antimicrobial cationic amphiphile functionalized mesocellular silica foam prepared on hard template/support activated carbon for enhanced simultaneous removal of Cu (II) and Zn(II) ions. J. Environ. Chem. Eng. 6, 4864–4877. https://doi.org/10.1016/j.jece.2018.07.029.

Tao, H.-C., Lei, T., Shi, G., Sun, X.-N., Wei, X.-Y., Zhang, L.-J., Wu, W.-M., 2014. Removal of heavy metals from fly ash leachate using combined bioelectrochemical systems and electrolysis. J. Hazard. Mater. 264, 1–7. https://doi.org/10.1016/j.jhazmat.2013.10.057.

Teng, W., Liu, G., Luo, H., Zhang, R., Xiang, Y., 2016. Simultaneous sulfate and zinc removal from acid wastewater using an acidophilic and autotrophic biocathode. J. Hazard. Mater. 304, 159–165. https://doi.org/10.1016/j.jhazmat.2015.10.050.

Ter Heijne, A., Liu, F., van der Weijden, R., Weijma, J., Buisman, C.J.N., Hamelers, H.V.M., 2010. Copper recovery combined with electricity production in a microbial fuel cell. Environ. Sci. Technol. 44, 4376–4381. https://doi.org/10.1021/es100526g.

Tombácz, E., 2009. Ph-dependent surface charging of metal oxides. Period. Polytech. Chem. Eng. 53, 77–86. https://doi.org/10.3311/pp.ch.2009-2.08.

W.F.D (WFD) U.K. TAG, U.K.T.A.G. on the W.F. Directive, Updated Recommendations on Environmental Standards, River Basin Management (2015–21): Final Report, 2013.

Wang, X., Li, J., Wang, Z., Tursun, H., Liu, R., Gao, Y., Li, Y., 2016a. Increasing the recovery of heavy metal ions using two microbial fuel cells operating in parallel with no power output. Environ. Sci. Pollut. Res. 23, 20368–20377. https://doi.org/10.1007/s11356-016-7045-y.

Wang, X., Li, J., Wang, Z., Tursun, H., Liu, R., Gao, Y., Li, Y., 2016b. Increasing the recovery of heavy metal ions using two microbial fuel cells operating in parallel with no power output. Environ. Sci. Pollut. Res. 23, 20368–20377. https://doi.org/10.1007/s11356-016-7045-y.

Wang, Y., Chen, Y., Wen, Q., 2018. Microbial fuel cells: enhancement with a polyaniline/carbon felt capacitive bioanode and reduction of Cr(VI) using the intermittent operation. Environ. Chem. Lett. 16, 319–326. https://doi.org/10.1007/s10311-017-0678-3.

Wu, J., Wang, Y., Zhang, D., Hou, B., 2011. Studies on the electrochemical reduction of oxygen catalyzed by reduced graphene sheets in neutral media. J. Power Sources 196, 1141–1144. https://doi.org/10.1016/j.jpowsour.2010.07.087.

Yu, J., Huang, T., Jiang, Z., Sun, M., Tang, C., 2018. Synthesis and characterizations of zinc oxide on reduced graphene oxide for high performance electrocatalytic reduction of oxygen. Molecules. 23, 3227. https://doi.org/10.3390/molecules23123227.

Zhang, L.-J., Tao, H.-C., Wei, X.-Y., Lei, T., Li, J.-B., Wang, A.-J., Wu, W.-M., 2012. Bioelectrochemical recovery of ammonia–copper(II) complexes from wastewater using a dual chamber microbial fuel cell. Chemosphere. 89, 1177–1182. https://doi.org/10.1016/j.chemosphere.2012.08.011.

Zhang, Y., Yu, L., Wu, D., Huang, L., Zhou, P., Quan, X., Chen, G., 2015. Dependency of simultaneous Cr(VI), Cu(II) and Cd(II) reduction on the cathodes of microbial electrolysis cells self-driven by microbial fuel cells. J. Power Sources 273, 1103–1113. https://doi.org/10.1016/j.jpowsour.2014.09.126.

Zhao, X., He, X., Chen, B., Yin, F., Li, G., 2019. MOFs derived metallic cobalt-zinc oxide@nitrogen-doped carbon/carbon nanotubes as a highly-efficient electrocatalyst for oxygen reduction reaction. Appl. Surf. Sci. 487, 1049–1057. https://doi.org/10.1016/j.apsusc.2019.05.182.